Analysis and Comparison of Transonic Buffet Phenomenon over Several Three-Dimensional Wings

E. Paladini,* J. Dandois,† and D. Sipp‡
DAAA, ONERA, Université Paris Saclay, 8 rue des Vertugadins, 92190 Meudon, France
and
J.-Ch. Robinet§
DynFluid Laboratory, Arts et Métiers ParisTech, 75013 Paris, France

The transonic buffet is a complex aerodynamic instability that appears on wings and airfoils at a high subsonic Mach number and/or angle of attack. It consists of a shock oscillation that induces pressure and notably lift fluctuations, thus limiting the flight envelope of civil aircraft. The aim of the present Paper is to improve the understanding of the flow physics of the three-dimensional transonic buffet over swept wings through the analysis and comparison of four different experimental databases. In particular, the objective is to identify characteristic values of the phenomenon such as Strouhal numbers, convection velocities, buffet onset, etc. It is shown that some dimensionless numbers are kept constant among the different databases and consequently can be considered as characteristics, whereas others change. The key factors in the understanding of the three-dimensional transonic buffet phenomenon lie in explaining common features but also the variability of transonic buffet characteristics in different configurations. In particular, it is shown that three-dimensional buffet is characterized by a Strouhal number in the range 0.2–0.3 and a spanwise convection velocity of $(0.245 \pm 0.015)U_\infty$, where U_∞ denotes the freestream velocity. These characteristic ranges of frequencies are larger than those of the two-dimensional buffet phenomenon, which suggests different physical mechanisms.

Nomenclature

a	=	speed of sound, $\mathrm{m \cdot s^{-1}}$
b	=	model span, m
c	=	local chord length, m
f	=	frequency, Hz
k	=	wave number, $\mathrm{m^{-1}}$
L	=	characteristic length, m
M	=	Mach number, U/a
MAC	=	mean aerodynamic chord, m
Re_{MAC}	=	Reynolds number based on mean aerodynamic chord
St	=	Strouhal number, fL/U_∞
U_c	=	convection velocity, $\mathrm{m \cdot s^{-1}}$
U_g	=	group velocity, $\mathrm{m \cdot s^{-1}}$
U_p	=	phase velocity, $\mathrm{m \cdot s^{-1}}$
U_∞	=	freestream velocity, $\mathrm{m \cdot s^{-1}}$
x, y, z	=	spatial coordinates, m
α	=	angle of attack, deg
β	=	convection velocity angle, deg
Λ	=	wing sweep angle, deg
$\Lambda_{x/c}$	=	angle of sensor line with respect to y axis, deg
λ	=	wavelength, m

I. Introduction

ON CIVIL aircraft, during cruise flight, a shock wave is present on the upper side of the wing. If the Mach number and/or the angle of attack is increased beyond a limit, a separation appears downstream of the shock. This separation leads to an instability of the shock-wave/boundary-layer interaction called transonic buffet. The shock position starts to oscillate in synchronization with the detachment/reattachment of the boundary layer, which results in large pressure fluctuations. If coupled with a structural mode, integral aerodynamic forces and moment fluctuations lead to structural vibrations of the entire wing, called buffeting. These vibrations can weaken the structure of the wings and in the worst case cause failure due to fatigue. Consequently, the buffet phenomenon limits the flight envelope of civil aircraft. During the wing design phase of an aircraft, buffet onset is evaluated just by empirical criteria (kink on the lift curve, divergence of the trailing edge pressure, etc.) and the experience coming from previous aircraft. In particular, the knowledge of the unsteady loads is a crucial point. Wind-tunnel tests on models at atmospheric conditions are generally not fully realistic because of the smaller Reynolds number, while the flight tests are complete but are available too late and are too expensive. This is the reason why computational fluid dynamics is gaining increasing importance. The objective of the aircraft manufacturers is to delay the value of buffet onset, which would lead to an improvement of aircraft aerodynamic performance (increase of the maximum takeoff weight, range, decrease of the wing area, etc.).

The first studies on buffet were conducted during and after World War II, when, thanks to technology evolution, aircraft reached transonic velocities. The aeronautical community started performing tests focused on a better understanding of transonic buffet in order to prevent potential structural damages and failure. Specifically, the tests were more focused on its control than on the understanding of the instability. The works really devoted to the understanding of the buffet physics were published only later and were first focused on two-dimensional (2D) airfoils. Actually, the phenomenon is not completely understood, and there are two main physical mechanisms to explain 2D transonic buffet. The first one, proposed by Lee [1], consists of a self-sustained loop based on the coupling between the shock and the trailing edge (TE) through pressure waves (see Fig. 1). The shock generates pressure waves, which propagate downstream inside the boundary layer. These waves are scattered at the TE, generating new waves that travel backward outside the boundary layer up to the shock. The numerical studies of Deck [2] and Memmolo et al. [3] suggest that the waves propagating downstream

*Ph.D. Student, Department of Aerodynamics, Aeroelasticity and Acoustics; edoardo.paladini@onera.fr.
†Ph.D., Department of Aerodynamics, Aeroelasticity and Acoustics; julien.dandois@onera.fr.
‡Professor, Department of Aerodynamics, Aeroelasticity and Acoustics; denis.sipp@onera.fr.
§Professor; Jean-Christophe. Robinet@ensam.eu.

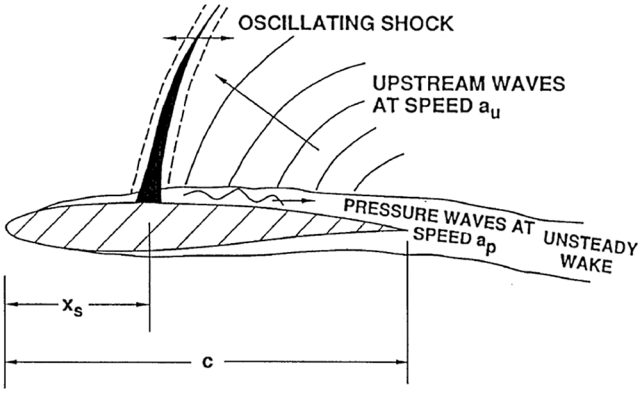

Fig. 1 Model of self-sustained shock oscillations from [1]; x_s is the shock position, and c is the chord.

are hydrodynamic waves while those propagating upstream are acoustic waves. Memmolo et al. describe all the possible acoustic rays displaying the right frequency, which are emitted at the TE and hit the shock front halfway of the sonic line. Deck and Xiao et al. [4] evaluated the propagation time from the shock wave to the TE; the value agrees well with the experimental one. The path of the closed-loop model is not completely established; in some cases, upstream pressure waves were visualized even on the lower side of the airfoil [5], which could suggest an alternative path for the closed loop. The second physical explanation comes from the stability analysis by Crouch et al. [6], in which the buffet instability is explained through an unstable global mode. Unstable global modes are coherent spatiotemporal fluctuations. These are generated by a self-sustained process as well, but here the pressure fluctuations appear downstream of the shock foot and move upward around the shock [7]. An unstable global mode is not the only way to explain an instability. Even when the entire spectrum exhibits stable modes, the instability could be explained with a noise amplifier mechanism; the unsteadiness is then due to the selective response of the flow to environmental forcing. The stability analysis of Crouch et al. has been repeated by Sartor et al. [8] and Guiho [9]. The results show good agreement among them on the values of the buffet frequency, growth rate, and description of the phenomenon at different $M - \alpha$ values: the buffet onset, the well-established buffet, and the buffet exit. Memmolo et al., after proposing a precise path for Lee's model consistent with the buffet frequency, performed a filtering of the acoustic field and showed that the buffet instability is either highly localized around the shock as observed by Crouch et al. [7] or connected with the separation bubble dynamics. More recently, Timme and Thormann [10] performed a three-dimensional (3D) global stability analysis on a half wing/body configuration, by using the same approach as the one used by Crouch et al. [6]. The emergence of a weakly damped global mode is found in the range $\alpha = 2$–3 deg, but no unstable mode has been found. Indeed, this kind of analysis in three dimensions is very interesting because it gives the possibility of understanding if the 3D transonic buffet phenomenon is due to an unstable global mode like in two dimensions or if it comes from a different physical nature.

The different flow physics between 2D and 3D buffet has been pointed out by several authors (Reneaux et al. [11], Roos [12], Molton et al. [13], and Dandois [14]). The frequency spectrum of 2D transonic buffet exhibits a well-marked peak (Jacquin et al. [5]), while the 3D spectrum is characterized by a broadband bump [12]. A dimensionless frequency, the Strouhal number, is introduced to compare results at different flow conditions and model sizes: $St = fL/U_\infty$ with f the buffet frequency, U_∞ the freestream velocity, and L the reference length, which is normally the chord in two dimensions and the mean aerodynamic chord (MAC) in three dimensions. The typical value of the Strouhal number is around 0.2–0.6 in 3D buffet, while it is around 0.05–0.07 in two dimensions. This means that the buffet frequencies are four to ten times higher in three dimensions than in two dimensions. The shock oscillation amplitude in two dimensions is about ten times larger than in three dimensions: from 20 to 2% of the chord for a well-established buffet. Another difference is found at higher values of the Mach number or the angle of attack: the amplitude of the shock oscillation in 2D buffet decreases until reaching a steady state. This phenomenon is known as buffet offset [8,15,16]. Sugioka et al. [17], Lawson et al. [18], and Koike et al. [19] performed experimental tests at high $M - \alpha$, but the same effect was not observed for the 3D buffet.

The early studies conducted on 3D configurations were mainly experimental. Hwang and Pi [20] presented an analysis of power spectral density (PSD) distributions obtained with unsteady pressure transducers during flight tests of a Northrop F-5A aircraft. The spectra showed a Strouhal number of about 0.23 for 3D buffet at well-established buffet conditions, but globally, the study was more focused on structural response. The description of the spectral content was then largely improved by Roos [12] for a high-aspect-ratio swept half-wing at Mach number 0.827 and an angle of attack of 11 deg. The heavy buffet regime presented a large bump in the pressure spectrum for the Strouhal number range 0.2–0.6. Eckstrom et al. [21,22] presented a complete study of mean pressure coefficients and unsteady pressure signals for different Mach numbers but without the analysis of the spectral content. More recently, unsteady pressure-sensitive paint (PSP) has been successfully used by Steimle et al. [23], Merienne et al. [24], Sugioka et al. [17], and Lawson et al. [18] to analyze the unsteady flowfield for transonic buffet over a transport-type swept wing. The model studied by Steimle et al. was flexible, and results exhibited important aeroelastic effects. The PSP measurements of Merienne et al. over a rigid model showed fairly good agreement with Kulite transducers. A new fast-responding PSP has been tested by Sugioka et al. over an 80%-scale model of the NASA Common Research Model (CRM). The results show a typical Strouhal number in the range 0.19–0.25 for $M = 0.85$ and an angle of attack between 4.2 and 6.8 deg. Lawson et al. presented in detail, together with unsteady PSP measurements, several buffet onset criteria. They defined two ranges of Strouhal numbers at a Mach number of 0.8: 0.08–0.16 for $\alpha = 2.8$ deg and 0.22–0.43 for $\alpha = 4$ deg. The same campaign was then analyzed by Masini et al. [25] by using proper orthogonal decomposition (POD) of the PSP measurements as well as flow control by vortex generators (VGs). POD modes showed the dominant structures of the flow: the structural response of the model and the shock unsteadiness across the span. Furthermore, a convection velocity of $0.26U_\infty$ was found on the wing at the buffet frequency.

Two campaigns, analyzed in the present Paper, have already been presented in previous studies. Molton et al. [13] showed the spectral analysis and results of buffet control by VGs for the ONERA research project BUFET'N Co. Dandois [14] performed a complete analysis of BUFET'N Co and AVERT databases. He gave values for the buffet onset at different values of $M - \alpha$ and characterized the frequency spectra evolution in the chordwise and spanwise directions. By using different signal processing tools, the convection velocities of the buffet phenomenon and of the Kelvin–Helmholtz (K–H) instability were obtained. A large-range investigation of $M - \alpha$ has been analyzed by Koike et al. [19]. A classification of the shock-wave oscillation in three regions was proposed. The first region is before buffet onset and without separation. The second region is the classical buffet phenomenon with a bump in the spectra at a Strouhal number around 0.3. The third region is at high $M - \alpha$ with large shock oscillations and a broadband bump in the spectra at low frequency. The results of the present Paper are entirely in the second region as defined by Koike et al. However, a behavior coherent with the third region is found: the bump in the spectra broadens and the frequency decreases when increasing α. Recently, Giannellis et al. [26] reviewed the developments and achievements in the understanding of the transonic buffet phenomenon. In the conclusions on the 3D buffet, they pointed out the main objective for future research on this topic: "to gain a comprehensive understanding of geometric effects" [26].

With the increase of computational resources, more and more unsteady numerical simulations of 3D configurations are performed. These simulations give a better overview of the overall three-dimensional flowfield, allowing comparison with experimental data and filling the lack of model instrumentation in all the experiments. The timescale of the periodic motion in transonic buffet is much longer

in comparison with the small-scale, high-frequency fluctuations of wall-bounded turbulence. Consequently, the unsteady Reynolds-averaged Navier–Stokes (URANS) equations approach, closed with a turbulence model, is better justified. Nevertheless, more expensive detached eddy simulations (DESs) have been used to compute the transonic buffet phenomenon. In DES, the attached boundary layer and regions where the turbulent length scale is smaller than a value fixed a priori are solved using the Reynolds-averaged Navier–Stokes approach while the other regions are directly resolved. Brunet and Deck [27], to the author's knowledge, were the first to perform a high-fidelity zonal DES (see the work by Deck [28] for more details) of the 3D transonic buffet phenomenon. They showed a good prediction of the time-averaged field compared with experiments. The same high-fidelity simulation was repeated by Deck et al. [29], showing the latest developments and trends for unsteady civil aircraft applications. Lutz et al. [30]also found good agreement between a new kind of zonal DES and experiments in the European Transonic Windtunnel (ETW) over the NASA CRM. Results showed a precise description of the unsteady development of the massively separated wing flow. More recently, Iovnovich and Raveh [31] and Sartor and Timme [32,33] performed URANS simulations of the transonic buffet. Iovnovich and Raveh studied the phenomenon on 3D wings at different sweep angles and aspect ratios. They were the first to give an interpretation of the path from 2D to 3D buffet. At zero or small sweep angles, the results are similar to the 2D phenomenon. When the sweep is increased, the Strouhal number also increases and reaches typical values of the 3D phenomenon with spanwise-propagating waves appearing on the wing, called buffet cells. This convective phenomenon was then observed in experiments. Dandois [14] computed for this the convection velocity by using a cross-spectrum analysis in the spanwise direction. These buffet cells are typical of the 3D transonic buffet. Sartor and Timme [32] also observed these complex structures in the spanwise direction typical of the 3D buffet. They studied the effects of different parameters such as the Mach number, angle of attack, and turbulence model on URANS simulations. Furthermore, in the work by Sartor and Timme [33], a comparison between delayed-DES and URANS simulations was presented, and even though delayed DES obviously showed a deeper description of the flow, good agreement of the main features of the flow was found with URANS modeling.

The link between 2D and 3D transonic buffet is a relevant question today, as is the impact of aerodynamic parameters, such as the Mach number, angle of attack, Reynolds number, etc., on different wings. A physical model explaining both kinds of buffet and the transition between them is a challenging objective. The present Paper is a continuation of the Molton et al. [13] and Dandois [14] ones. The first is more oriented toward buffet control, while the second is based on two wind-tunnel tests and oriented toward the analysis of the phenomenon. Here, two additional databases are investigated, and new spectral analyses are performed. The main objective is the definition of characteristic values of dimensionless numbers like the Strouhal number and the analysis of the variability of transonic buffet with the flow conditions or the wing geometry.

The Paper is organized as follows. Section II defines the experimental setup used in each database. Buffet onset for the four wind-tunnel tests is described in Sec. III. Section IV gives information on the evolution of the separated zone with the flow conditions. In Sec. V, a spectral analysis of the Kulites data is performed. In Sec. VI, signal processing tools like cross-spectra and frequency-wave number spectra of the Kulites data are used to compute convection velocities of the buffet phenomenon. Finally, the conclusion presents a synthesis of the results with physical discussions and perspectives.

II. Experimental Setup

In the present Paper, four different campaigns are analyzed and compared. These campaigns were performed in three wind-tunnel tests with four different half wing-body configurations. They correspond to the following projects:

1) An ONERA research project called BUFET'N Co was launched in 2007 in the ONERA S3Ch wind tunnel over a half wing-body configuration based on the OAT15A airfoil (Fig. 2a).

2) A European project called AVERT was launched in 2007 in the ONERA S2MA wind tunnel over a half wing-body configuration based also on the OAT15A airfoil (Fig. 2b).

3) A French project called DTP Tremblement was launched in 2004 in the ONERA S2MA wind tunnel over a half wing-body Dassault Aviation model (Fig. 2c).

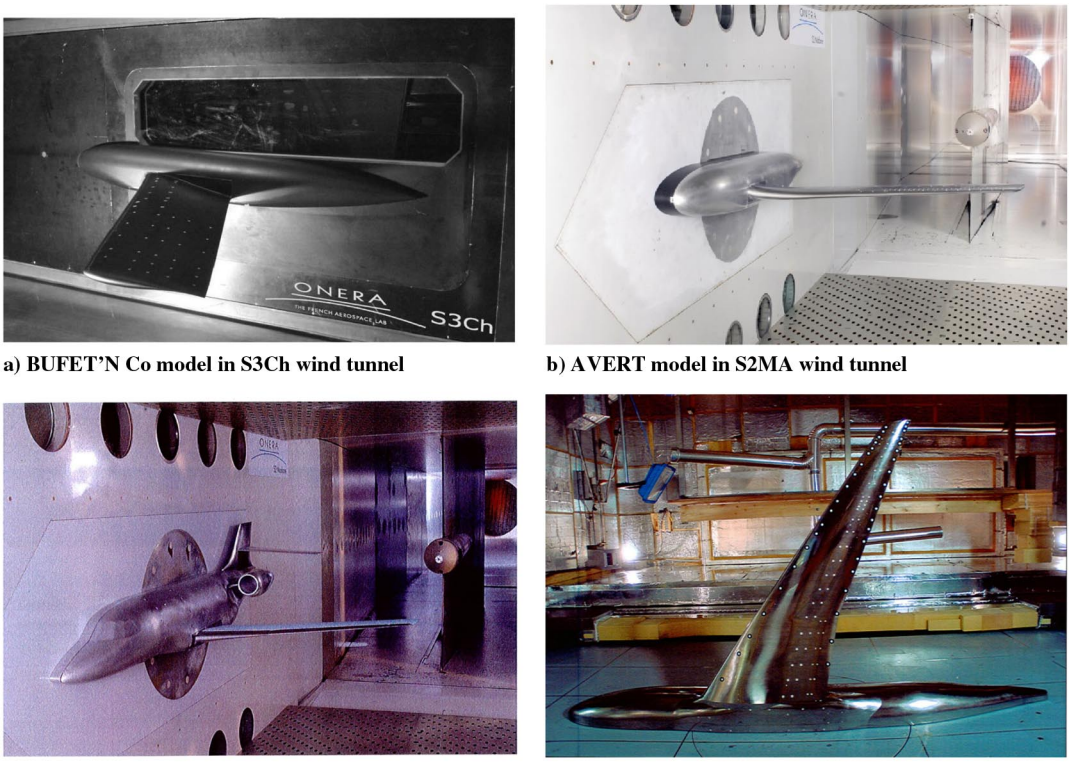

a) BUFET'N Co model in S3Ch wind tunnel

b) AVERT model in S2MA wind tunnel

c) DTP Tremblement model in S2MA wind tunnel

d) FLIRET model in ETW

Fig. 2 Overview of the four models inside their respective wind tunnels.

4) A European project called FLIRET was launched in 2005 in the ETW over a half wing-body Airbus model (Fig. 2d).

Figure 2 shows pictures of the four models inside their corresponding wind tunnels, and Fig. 3 shows the locations of the equipment on the suction side of the wing and the orientation of the reference frame with respect to each model. In the following paragraphs, the three wind tunnels and the four models are presented.

S3Ch is a continuous closed-circuit transonic wind tunnel in the ONERA Meudon center. The test section size is $0.76 \times 0.82 \times 2.2$ m. The stagnation pressure is the atmospheric one, and the stagnation

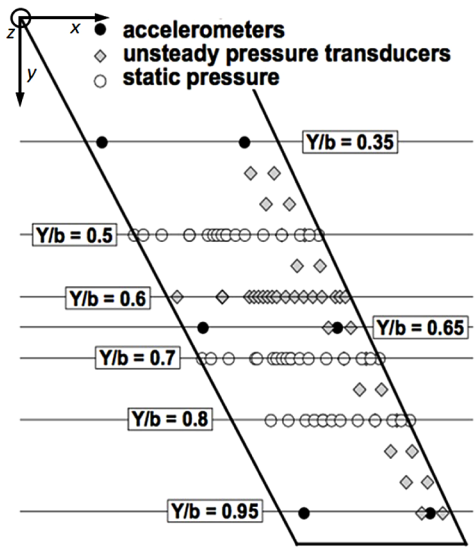

a) BUFET'N Co

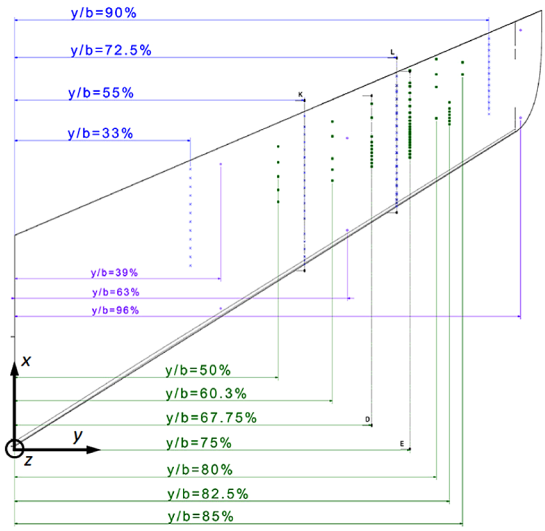

b) AVERT: static pressure in blue, unsteady pressure transducers in green, and accelerometers in purple

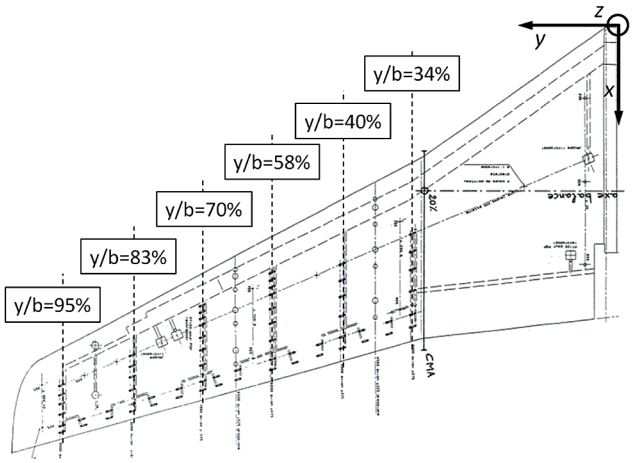

c) DTP Tremblement: unsteady pressure transducers in black points

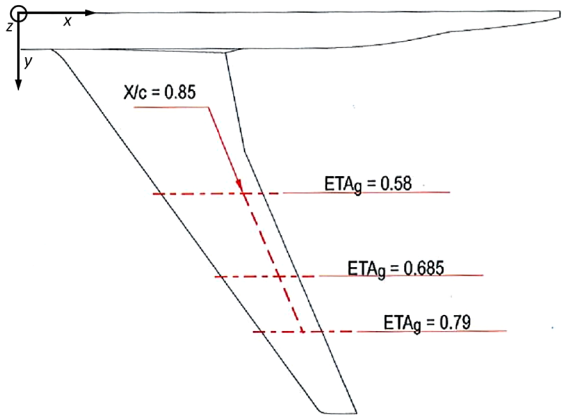

d) FLIRET: four lines of unsteady pressure transducers in red

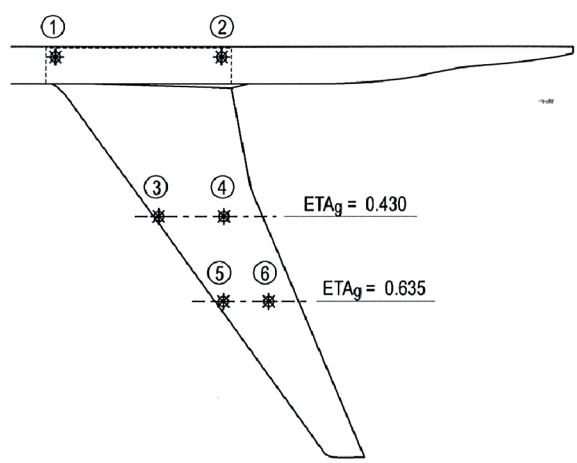

e) FLIRET: six accelerometers in black

Fig. 3 Models equipment.

Table 1 Summary of the experimental conditions for the four databases

Databases	BUFET'N Co	AVERT	DTP Tremblement	FLIRET
Re_{MAC}	2.5×10^6	$2.83–8.49 \times 10^6$	$2.02–6.25 \times 10^6$	$23.5–70.5 \times 10^6$
M	0.82	0.78–0.86	0.75–0.85	0.85–93
α, deg	2–4	0–6.5	2.5–4.5	−0.5 − 6.5
Boundary-layer tripping (x/c)	7%	7%	10%	No trip
MAC, m	0.22	0.3375	0.251	0.384
MAC′, m			0.193	0.264
b, m	0.704	1.225	0.943	1.3167
Sampling rate (Kulites, accelerometers), Hz	20480	2048	2048	4096
Anti-aliasing filter, Hz	9216	921.6	750	819
Nb overlapping blocks	65	127		62
Frequency resolution, Hz	8	2	25	2
Frequency resolution (St_{MAC})	0.0063	0.0024	0.023	0.0038

temperature lies between 290 and 310 K. The shapes of the upper and lower walls are adapted for each flow condition based on a steady flow hypothesis so as to reproduce far-field conditions. The S2MA wind tunnel of the ONERA Modane-Avrieux center is a continuous pressurized subsonic/transonic/supersonic wind tunnel. The test section size is 1.765×1.75 m. Upper and lower walls are perforated in order to reduce their influence on the flow. The ETW located in Cologne, Germany, is an industrial cryogenic pressurized facility. The ETW has a closed aerodynamic circuit with a test section size of $2 \times 2.4 \times 8.73$ m.

The BUFET'N Co model (Fig. 2a) is composed of a swept wing attached on a half-fuselage, the sweep angle at the leading edge (LE) is 30 deg, and the wing is based on the supercritical OAT15A airfoil. From root to tip, the chord varies between 0.24 and 0.2 m. Consequently, the MAC is equal to 0.22 m. The model is equipped with 49 static pressure taps, 39 unsteady Kulite pressure transducers, and 6 accelerometers (Fig. 3a). The AVERT model is a simplified half wing-body configuration. Most of the wing profile is based on the OAT15A airfoil like the BUFET'N Co model. The sweep angle at the LE is 30 deg. The chord length is 0.450 m at the wing root and 0.225 m at the wing tip, resulting in a MAC of 0.3375 m. Tests were performed for different stagnation pressure values (from 0.6 up to 1.8 bar). Many steady pressure taps and unsteady pressure transducers were installed on the model: 86 pressure taps on four wing sections, 65 on the upper and 21 on the lower surface of the wing; 57 unsteady pressure transducers on seven wing sections, 53 on the upper and 4 on the lower surface of the wing; and three wing sections with two accelerometers each (Fig. 3b). The DTP Tremblement model, tested in S2MA as the AVERT model, is a half wing-body configuration defined by Dassault Aviation. It is based on a supercritical airfoil with a double-sweep wing. The value of the MAC is 0.251 m, and because the model is a double-sweep wing, a second mean aerodynamic chord based only on the external sweep part of the wing is defined $\mathrm{MAC}' = 0.193$ m. For this project, the data are already treated, so only the power spectral densities, the correlations between couples of sensors, and rms of Kulites are available. The model is equipped with 62 Kulites (all in the outboard part of the wing, Fig. 3d). Finally, the FLIRET model is a half wing-body configuration defined by Airbus UK. It is a typical Airbus model with a supercritical airfoil and a double sweep at the trailing edge. The MAC is 0.348 m, and $\mathrm{MAC}' = 0.264$ m. The sweep angle at the leading edge is 30 deg. The model is equipped with 42 Kulites and six accelerometers (Fig. 3c). Table 1 summarizes the experimental flow conditions for the four databases.

III. Buffet Onset

The definition of the range in which the buffet phenomenon appears is the first step in the analysis of experimental results. The values of the buffet onset are presented in this section. The buffet offset, defined in two dimensions [8,15,16] has not been observed. The four campaigns have not been designed to investigate the buffet offset; furthermore, the tests at high $M - \alpha$ do not reveal the presence of buffet offset.

Different buffet onset criteria are presented. The main difference is between local and global criteria. Global criteria are common methods used in the industry. They are based on the structural response of the wing or on the integral variables. Figures 4a and 4b show the analysis of the lift curve and the rms values of the accelerometer at the wing tip, respectively. Concerning the lift curve, the buffet onset is defined by the intersection between the lift curve and a straight line parallel to the linear part of the lift curve shifted by $+0.1$ deg. Concerning the analysis of the accelerometer, the buffet onset is defined in the present Paper when the rms value exceeds 1.4 times (defined empirically) the rest value. The two criteria agree well and give a buffet onset value of $\alpha \cong 3$ deg.

The local buffet criteria are based on the analysis of the mean pressure value at the trailing edge [34] or the rms of the unsteady pressure transducers [35]. These criteria have to be applied on each section of the wing in order to find in which section buffet appears first. The onset is defined when the static value of the pressure coefficient Cp at the trailing edge diverges more than 0.05 [34] or when the rms value exceeds 2.5 times (defined empirically) the initial plateau. It is possible to define an initial plateau because far before buffet onset the rms of Kulites is constant as clearly shown in Fig. 4c. Figures 4d and 4e do not show clearly the initial plateau because the α range is not large enough. For these cases, the value of the initial plateau is taken at $\alpha = 2.45$ and 2.25 deg, respectively, for which the value is close to the initial plateau (based on the comparison with other tests). The local criteria based on the rms of the Cp identify a buffet onset of $\alpha \cong 3.1$ deg for DTP Tremblement and $\alpha \cong 3$ deg for both BUFET'N Co and FLIRET.

Finally, Fig. 5 show the buffet onset for FLIRET and AVERT tests at different values of the Mach numbers. In Fig. 5a, the values of buffet onset have been identified by the three criteria presented in previous paragraphs, which are in agreement with each other. Figure 5b from Dandois [14] identifies the buffet onset at $\alpha \cong 3 \pm 0.1$ deg for the AVERT project at $M = 0.82$. In both tests, the higher the Mach number, the lower the angle of attack for which buffet onset occurs.

IV. Separated Flow Evolution

Oil flow visualizations are available for the BUFET'N Co and AVERT campaigns. Therefore, it is possible to describe the evolution of the separated flow on the suction side of the wing. Figure 6 shows five oil flow visualizations for the BUFET'N Co case at $M = 0.82$. The blue oil is coming from the pressure side, and consequently, the size of the blue area reveals the extension of the separated zone. Figures 6a and 6b at $\alpha = 2.5$ and 2.8 deg show a flow fully attached on the suction side of the wing with the exception of a zone at the wing tip caused by the vortex tip. In Fig. 6b, the shock moves upstream, and skin-friction lines tend to be parallel to the TE in the area of $y/b = 55\%$. The detached zone appears at buffet onset, and it is clearly revealed by Figs. 6c and 6d. In well-established buffet conditions at $\alpha = 3.5$ deg (Fig. 6e), the separation point moves toward the shock foot, and the separation zone spreads in span in both directions (inboard and outboard). Furthermore, the maximal value of unsteadiness at TE moves in span toward the wing tip.

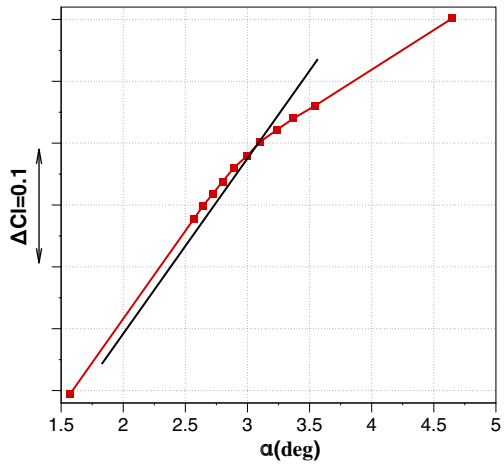

a) Lift curve for FLIRET project at M = 0.85

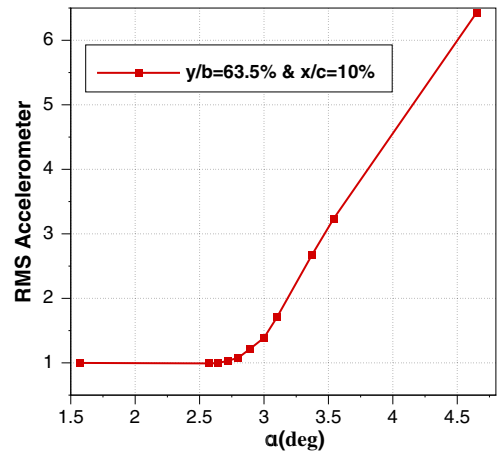

b) RMS of accelerometer close to the wing tip for FLIRET project at M = 0.85

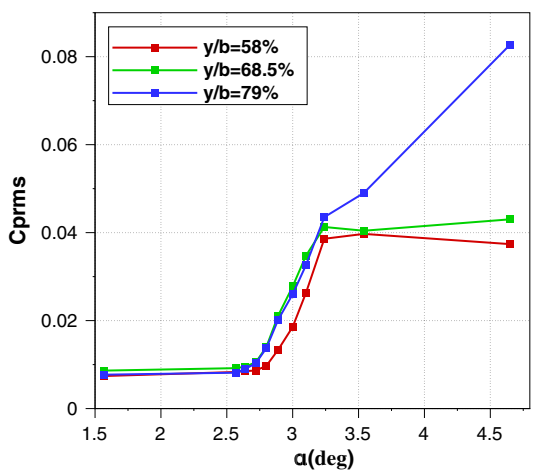

c) RMS of Kulites for FLIRET close to TE at M = 0.85

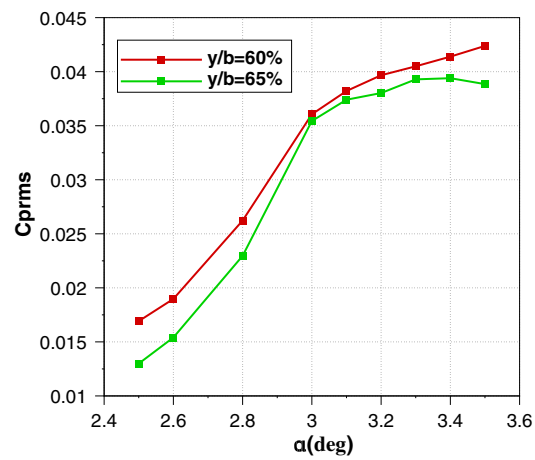

d) RMS of Kulites for BUFET'N Co close to TE at M = 0.82

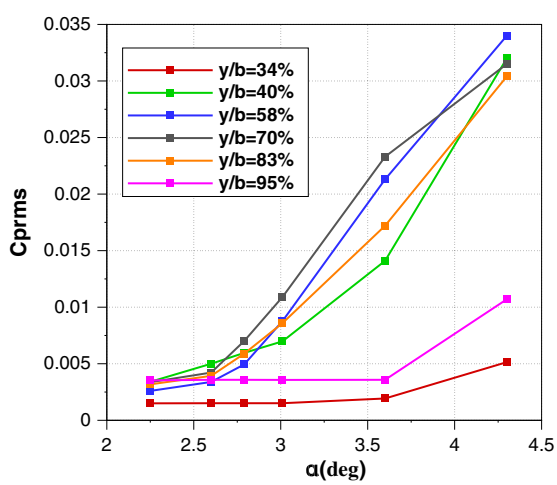

e) RMS of Kulites for DTP Tremblement close to TE at M = 0.8

Fig. 4 Buffet onset criteria.

The oil flow visualization of the AVERT test is shown in Fig. 7. Here, the oil coming from the pressure side is red. The separation appears for α approaching the buffet onset at about $y/b = 67.75\%$ (Fig. 7a). When α increases, the separation point moves, as for BUFFET'N Co, toward the shock foot and in span in both directions. Figure 7b shows the oil flow visualization at $\alpha = 3.5$ deg. The flow is separated between $y/b = 42.5\%$ and $y/b = 82.5\%$. Both visualizations show the detachment due to the vortex tip. The separated flow condition at a higher Mach number of 0.86 is similar (figures omitted). At $\alpha = 0$ deg, the flow is fully attached. When approaching buffet onset, a separated zone appears at about $y/b = 75\%$, i.e., more outboard than for $M = 0.82$.

V. Power Spectral Densities

The PSDs of Kulites data are presented in this section. PSDs are computed with the same procedure as in the work by Dandois [14]: Welch's method with Hamming window and 50% overlapping

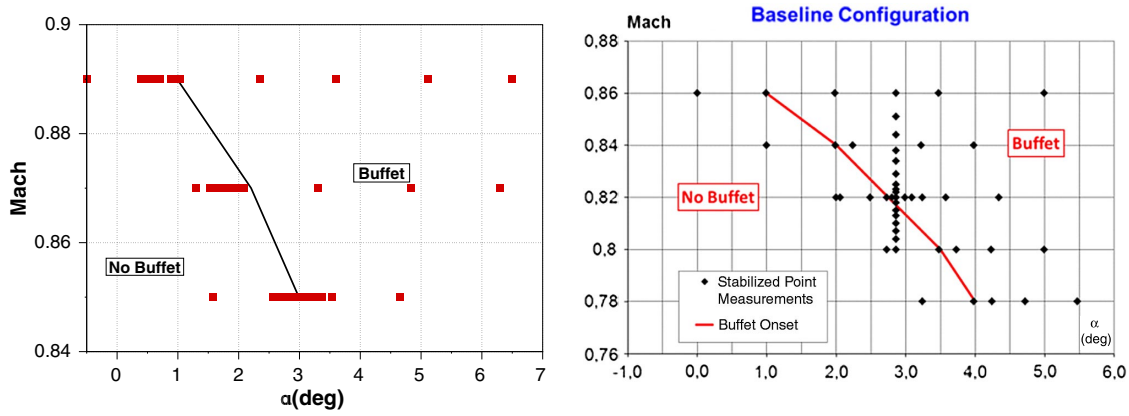

a) FLIRET tests

b) AVERT tests from Dandois [14]

Fig. 5 Buffet onset limit in the M–α plane.

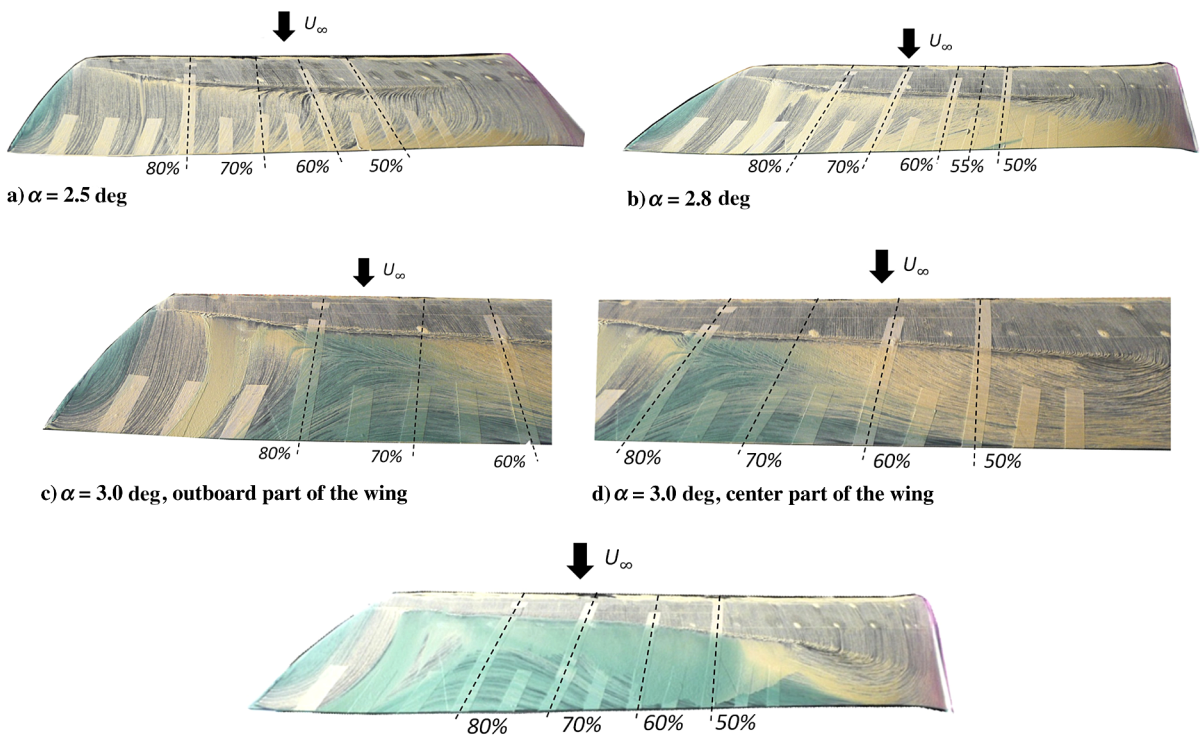

a) $\alpha = 2.5$ deg

b) $\alpha = 2.8$ deg

c) $\alpha = 3.0$ deg, outboard part of the wing

d) $\alpha = 3.0$ deg, center part of the wing

e) $\alpha = 3.5$ deg

Fig. 6 Oil visualizations for BUFET'N Co test at $M = 0.82$ for increasing values of α.

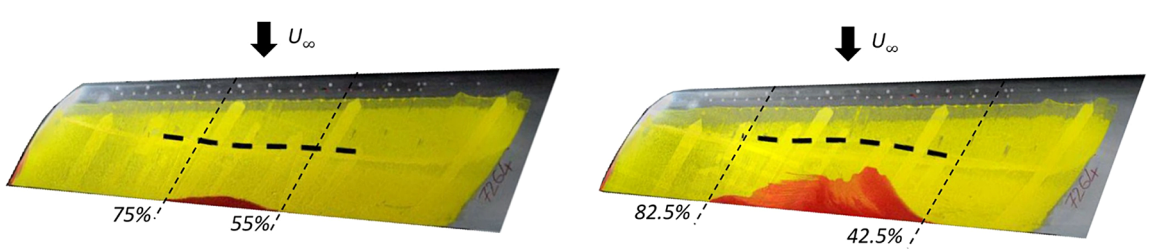

a) $\alpha = 3$ deg

b) $\alpha = 3.5$ deg

Fig. 7 Oil flow visualization for AVERT test at $M = 0.82$. The thick dashed line shows the shock location.

blocks. The number of overlapping blocks and the frequency resolution are given in Table 1 for each campaign. As already stated, the main difference between 2D and 3D buffet is the increase of shock frequency oscillation and the broadening of the buffet frequency range. Consequently, the identification of a precise value of buffet frequency is more complicated in three dimensions than in two dimensions, in which the PSD exhibits clear peaks. Nevertheless, it has been chosen to define the buffet frequency as the center of gravity of these bumps. The PSDs are analyzed on the whole wing, i.e., in the chordwise (iso-x/c) and spanwise (iso-y/b) directions, in order to get the spatial variations of the buffet frequency. The PSDs, depending on the frequency sampling, can also show other physical phenomena. The K–H instability appears in the frequency range 1000–4000 Hz. The theoretical frequency is around $f_{\text{K–H}} = 0.135\bar{U}/\delta_\omega$, where $\bar{U}$ is

the average velocity above and below the shear layer and δ_ω is the vorticity thickness (see the work by Huerre and Rossi [36] for more details). The K–H phenomenon exists in every test, but spectra of AVERT, FLIRET and DTP Tremblement overlook the phenomenon due to a low-pass filter applied to each signal. Nevertheless, it is still possible to observe the K–H instability in the frequency-wave number spectra for the AVERT and FLIRET tests. This is because the frequency-wave number $(f-k)$ spectrum is based on signal coherence, so even if signals are filtered, large coherent zones remain. The dimensionless Strouhal number $St = (fL)/U_\infty$ has been defined to compare the results over different models. Three different lengths are considered here for L: the local chord, MAC, and MAC′. Consequently, three Strouhal numbers can be defined. The reason lies in the different points of view on the phenomenon: local or global in space. A local Strouhal number means an analysis only at a given section, so with the value of the chord at this section. The Strouhal number based on MAC tries to define a global value for the entire wing, as if there were an unstable global mode that synchronizes all sections. Furthermore, for wings with a high value of the taper ratio, it is compulsory to consider the local Strouhal number in order to perform comparisons with small taper ratios (like the FLIRET and BUFET'N Co tests).

A. PSDs for BUFET'N Co Model

BUFET'N Co tests are performed at a Mach number of 0.82, and α ranges from 2.5 to 3.5 deg. Figures 8a and 8b show the PSDs of Kulites data in the chordwise direction at $y/b = 60\%$ for the test cases at $\alpha = 3.2$ and 3.5 deg, respectively. The section at $y/b = 60\%$ has been chosen because it is the first where a separation at the TE appears and because it is the best equipped with sensors. The Kelvin–Helmholtz instability clearly appears in both spectra at its typical Strouhal number (1–4) when approaching the TE, because the flow is more separated (Fig. 6). The intensity of the K–H instability increases approaching the wing tip, except for the final flow reattachment due to the wing tip vortex (Figs. 6c and 6e). Close to the onset at $\alpha = 3.2$ deg, the bump in the spectra is very large and centered around $St_{\mathrm{MAC}} = 0.34$. Here, the variations of the buffet Strouhal number in the span and chord are very weak (it is even difficult to visualize the buffet peak when approaching the TE). At $\alpha = 3.5$ deg, corresponding to well-established transonic buffet conditions, the situation is relatively different. It is easier to identify a bump in the spectra, and the variations in the chordwise and spanwise directions are clearer. In the chordwise direction, the buffet Strouhal number decreases from around $St_{\mathrm{MAC}} = 0.34$ at $x/c = 60\%$ to $St_{\mathrm{MAC}} = 0.2$ at the TE. A spanwise variation of the buffet Strouhal number is observed with an oscillation between the critical section and the wing tip: it decreases up to $y/b = 60\%$ (where the K–H instability is the strongest) then increases before a final decrease at the wing tip. The map in Fig. 9 shows the overall variations of the buffet Strouhal number on the wing.

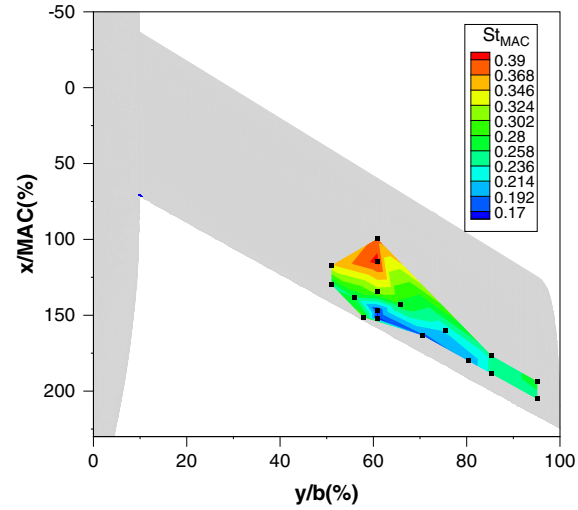

Fig. 9 Buffet Strouhal number map for BUFET'N Co test at $\alpha = 3.5$ deg and $M = 0.82$.

B. PSDs for AVERT Model

During the AVERT campaign, several values of α were tested at Mach numbers 0.78, 0.8, 0.82, 0.84, and 0.86. This database has already been analyzed by Dandois [14], so here the results are presented in comparison with the other databases. The analysis is focused on the tests performed at $M = 0.82$. Figures 10a and 10b show the map with values of buffet Strouhal numbers over the wing at $\alpha = 3.47$ and 4.99 deg, respectively. Typical values of buffet Strouhal numbers around $St_{\mathrm{MAC}} = 0.25$–0.27 are identified on the PSDs. In Fig. 10a, in well-established transonic buffet conditions, the Strouhal numbers strongly vary on the wing. Besides, as noted for the onset in BUFET'N Co, Fig. 10b shows smaller variations on the wing at higher incidence. Figure 10c shows two PSDs at the shock foot for $\alpha = 1.99$ and 3.47 deg. One can observe that the bump of the Strouhal number decreases with α. The same behavior is found at different values of the Mach number.

C. PSDs for DTP Tremblement Model

For this database, only rms values of the sensors signal, cross-spectra (coherence and phase), and PSDs are available. The resolution of these treatments in the frequency domain is 25 Hz ($St_{\mathrm{MAC}} = 0.023$ at $M = 0.8$), and the frequency range of analysis is

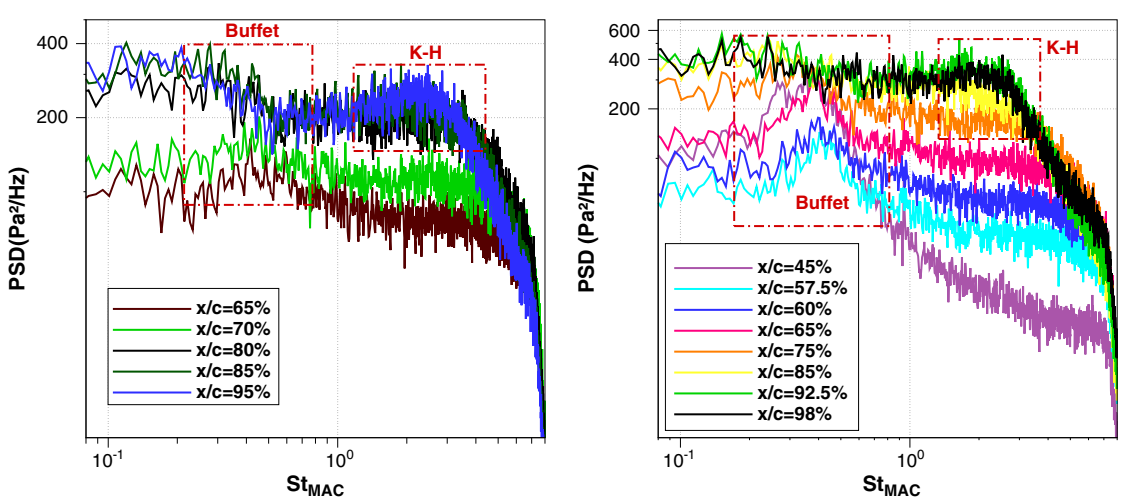

a) $\alpha = 3.2$ deg **b) $\alpha = 3.5$ deg**

Fig. 8 Log–log graph of power spectral densities for BUFET'N Co test at $M = 0.82$ in the chordwise direction at $y/b = 60\%$.

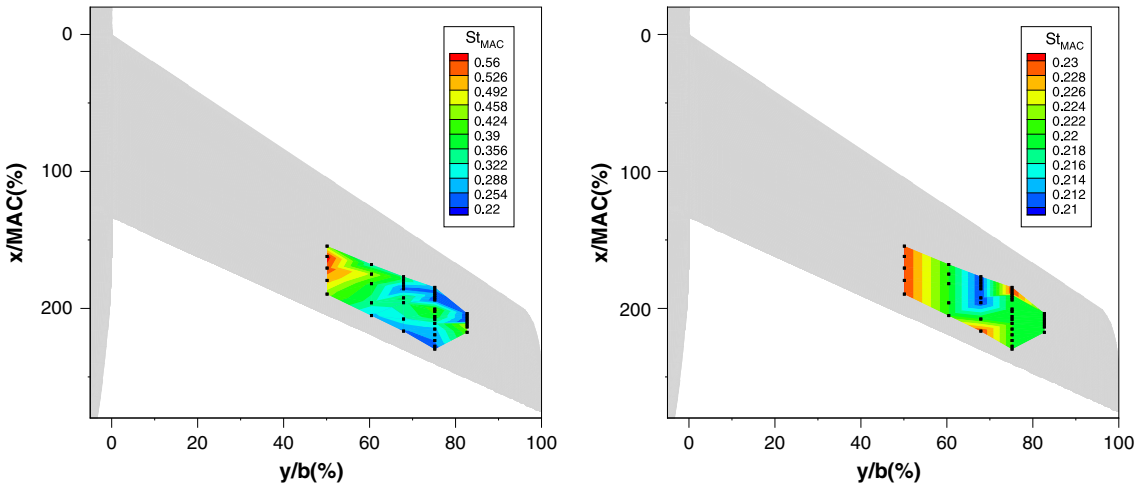

a) Buffet Strouhal number map at $\alpha = 3.47$ deg and $M = 0.82$ b) Buffet Strouhal number map at $\alpha = 4.99$ deg and $M = 0.86$

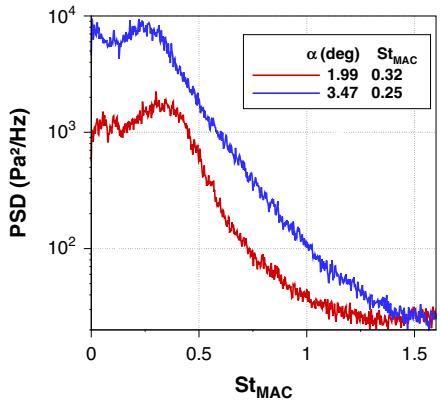

c) Semi-log graph of power spectral densities at shock foot and $y/b = 75\%$ for $M = 0.86$ with values of buffet Strouhal numbers in the legend

Fig. 10 PSDs for AVERT tests.

0–750 Hz ($St_{\mathrm{MAC}} = 0$–0.69 at $M = 0.8$), too low for the visualization of the K–H instability. Tested Mach numbers are 0.75, 0.8, 0.825, and 0.85 for various α. In particular, a series of tests at $M = 0.8$ with the nacelle, stabilizers, and boundary-layer transition fixed at 10% are analyzed. Here, a large range of buffet Strouhal numbers is found: from 0.28 to 0.36. The reasons for this large range is due to the large range of M–α analyzed and to the double-sweep geometry of the wing. Figures 11a and 11b highlight the difference in PSDs between well-established ($\alpha = 3.6$ deg) and deep buffet ($\alpha = 4.3$ deg) conditions at $y/b = 70\%$. In the first case, the buffet bumps are wide and slightly vary on the wing. A value of $St_{\mathrm{MAC}} = 0.28$ ($St = 0.19$ based on local chord and 0.22 based on MAC′) is found. At $\alpha = 4.3$ deg, it is easier to identify a bump at $St_{\mathrm{MAC}} = 0.21$ ($St = 0.14$ based on the local chord and 0.16 based on

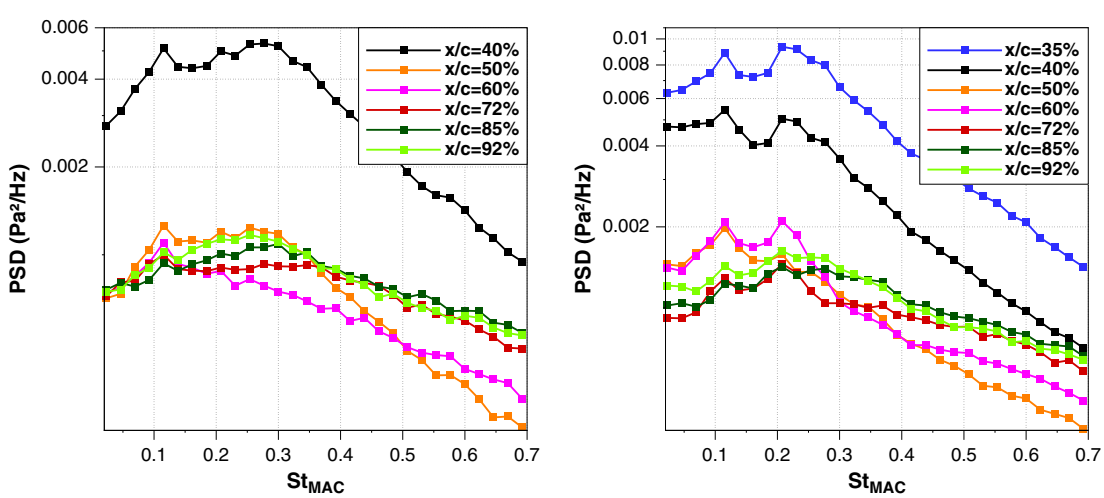

a) $\alpha = 3.6$ deg b) $\alpha = 4.3$ deg

Fig. 11 Semilog graph of power spectral densities for DTP Tremblement at $M = 0.8$ in the chordwise direction at $y/b = 70\%$.

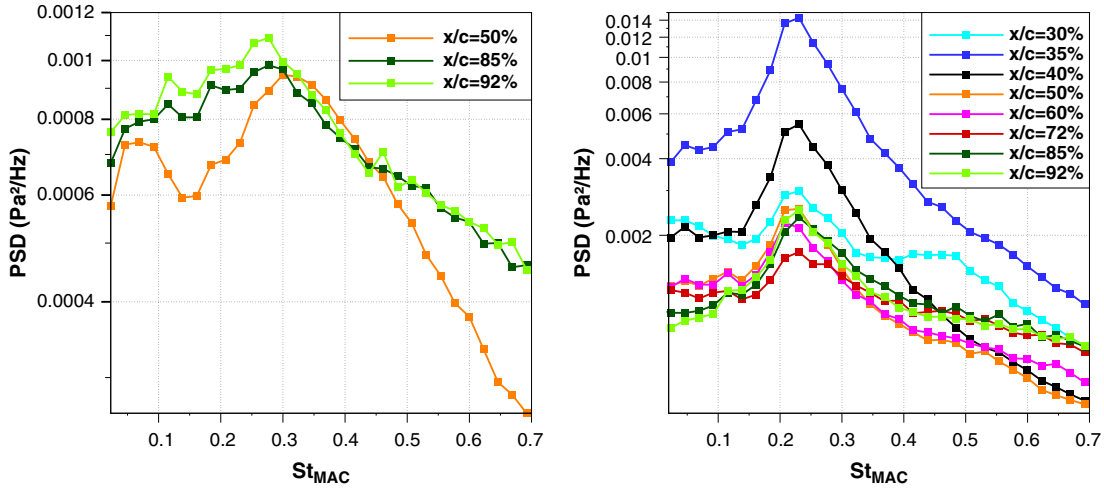

a) $\alpha = 3.6$ deg b) $\alpha = 4.3$ deg

Fig. 12 Semilog graph of power spectral densities for DTP Tremblement at $M = 0.8$ in the chordwise direction at $y/b = 58\%$.

MAC′). The figures show that the buffet Strouhal number decreases and bumps tend to become thinner when increasing α at a fixed Mach number. Figure 11 shows also a peak due to a structural mode ($St_{\mathrm{MAC}} = 0.12$). Similar behaviors are found in an inner section at $y/b = 58\%$ (Fig. 12). Buffet frequency clearly decreases in the chordwise direction at $\alpha = 3.6$ deg, while at $\alpha = 4.3$ deg, it remains more constant. In the same way, a comparison between Figs. 12a and 11a shows a decrease of the buffet bumps in the spanwise direction, from 0.28–0.32 to 0.25–0.28.

D. PSDs for FLIRET Model

Five values of the Mach number are considered (0.85, 0.87, 0.89, 0.91, and 0.93), while the angles of attack are taken to be centered around buffet onset. There is no transition triggering thanks to a cryogenic temperature of 162 K, which gives a sufficiently high Reynolds number to have a fully turbulent flow (using MAC as a reference length: 8.2×10^6 to 70.5×10^6). The FLIRET wind-tunnel test has the model with the lowest taper ratio (0.21) and the largest range of M–α (0.85–0.91/0.5–6.4 deg). Consequently, a large buffet Strouhal number range is found when analyzing the PSDs. It is possible to find values of St_{MAC} from 0.22 to 0.95. The lowest values of the buffet Strouhal number are usually found around the wing tip at high M–α. At buffet onset ($\alpha = 3$ deg), the buffet Strouhal number is roughly constant all over the wing around 0.65–0.8. In well-established buffet conditions (Figs. 13), variations of the buffet Strouhal number appear on the wing: it decreases toward the wing tip and a little in the chord as well. The variations in the chord are less clear than in the span, especially toward the wing tip (Fig. 14). The variations of the buffet Strouhal number in the wing direction (chord and span) and with α are the same as for the other models.

Comparing models with different geometries, it is important to identify the characteristic lengths that best fit the dimensionless numbers. Here, because of the low taper ratio of the model, the buffet Strouhal number based on the local chord length is preferred. In this case, the Strouhal number range of Fig. 13 is reduced to 0.2–0.35 with a characteristic value of 0.25 in $x/c = 85\%$ and $y/b = 79\%$. A comparison among the buffet Strouhal numbers based on the local chord and the two kinds of mean aerodynamic chords shows that the range of Strouhal numbers decreases from 0.5–0.8 (based on MAC) to 0.3–0.5 (based on MAC′) and finally 0.2–0.35 (based on the local chord).

VI. Cross-Spectral Analysis

In this section, signal processing tools are presented, like cross-spectra and frequency-wave number spectra. They are an efficient way to determine the convection velocities of the 3D buffet phenomenon (and of the K–H instability). U_{Cc} and U_{Cs} are the convection velocity components in the chordwise direction toward the TE and in the spanwise direction toward the wing tip, respectively; β is the angle between the wave propagation and the chordwise direction. U_{Cc} and U_{Cs} can be identified by two different analyses: cross-spectra and frequency-wave number spectra. Then,

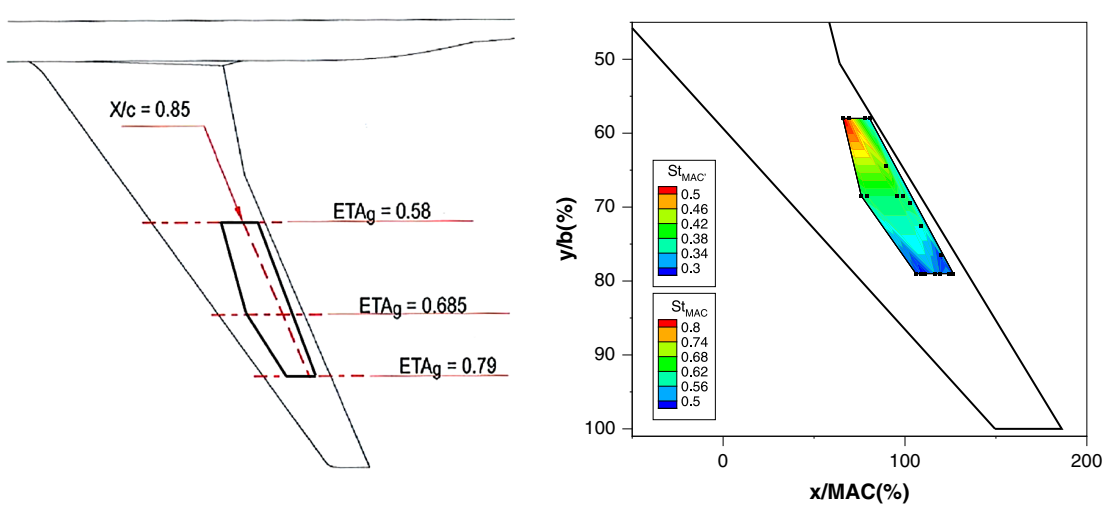

a) Definition of the analyzed zone on the model b) Buffet frequency map

Fig. 13 Buffet Strouhal number map for FLIRET test at $\alpha = 3.37$ deg and $M = 0.85$.

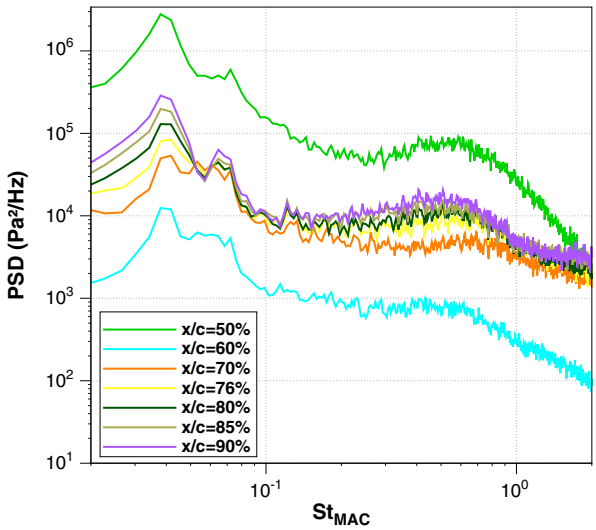

Fig. 14 Log–log graph of power spectral densities for FLIRET at $\alpha = 3.37$ deg and $M = 0.85$ in the chordwise direction at $y/b = 79\%$.

the resulting convection velocities U_C and the directions β are computed. These velocities are defined for a fixed value of frequency, or at least a range, in order to link the velocity to the physical phenomenon appearing at the considered frequencies.

A. Cross-Spectrum

The cross-spectrum is the Fourier transform of the cross-correlation of two stochastic processes: in the present case, the measured signals from the Kulites. If $x_1(t)$ and $x_2(t)$ are two continuous signals, the cross-correlation $R_{x_1x_2}(\tau)$ is the convolution of the signals:

$$R_{x_1x_2}(\tau) = \int_{-\infty}^{\infty} x_1(t)x_2(t+\tau)\,\mathrm{d}t \tag{1}$$

The Fourier transform $\mathcal{F}$ converts the cross-correlation $R_{x_1x_2}(\tau)$ from the time to the frequency domain, defining in this way the cross-spectrum $\hat{R}_{x_1x_2}(f)$:

$$\hat{R}_{x_1x_2}(f) = \mathcal{F}\{R_{x_1x_2}(\tau)\} = \int_{-\infty}^{\infty} R_{x_1x_2}(\tau)e^{-2i\pi f\tau}\,\mathrm{d}\tau \tag{2}$$

The cross-spectrum $\hat{R}_{x_1x_2}(f)$ in polar coordinates can be decomposed into an amplitude $\hat{A}_{x_1x_2}(f)$ and a phase $\Phi_{x_1x_2}(f)$. The latter is used to compute the convection velocity, while the square of the amplitude divided by the spectra of the two signals gives the coherence γ^2:

$$\hat{R}_{x_1x_2}(f) = \hat{A}_{x_1x_2}(f)e^{i\Phi_{x_1x_2}(f)} \tag{3}$$

$$\gamma^2_{x_1x_2}(f) = \frac{\hat{A}^2_{x_1x_2}(f)}{\hat{R}_{x_1x_1}(f) * \hat{R}_{x_2x_2}(f)} \tag{4}$$

The coherence allows identifying the range in the frequency domain where there are convective phenomena, and from the phase difference, it is possible to compute their velocities. Normally, there are high values of the coherence at the buffet Strouhal number. Then, there are two ways to estimate the convection velocities. The two methods are based on the same idea and give almost the same results. The first one consists of selecting the frequency for which the coherence is the highest and then looking at linear variations of the phase at this frequency in space. It is very precise in terms of frequency, while it is averaged in space. Convection velocity is obtained using the relation $U_C = 2\pi f\Delta x/\Delta\varphi$, where f is the selected frequency in hertz, Δx is the length of the line of sensors used in meters, and $\Delta\varphi$ is the phase difference in radians. The second method is computed specifically between two sensors. The range of frequencies with high coherence shows a linear variation of phase in the frequency domain. From this slope, it is possible to obtain the convection velocity, $U_C = 2\pi\Delta x\Delta f/\Delta\varphi$, where the variables are the same as previously expressed except for Δf, which here is a range and not a single value. This case is more precise in space because just two sensors are analyzed but averaged in the range of frequencies at which the coherence is maximal. This is the reason why it is important to consider only the frequency range of the interesting phenomenon. Figure 15 shows an example of the analysis of a cross-spectrum for two sensors of the BUFET'N Co test at $\alpha = 3.5$ deg and $M = 0.82$. It is possible to see that the coherence is high only in the buffet Strouhal number range, in which a linear slope is found in the phase plot. Finally, by combining the two velocities component in spanwise and chordwise directions, it is possible to compute the norm and direction of the resulting velocity vector. The chordwise and spanwise velocities are not combined in the classical vectorial way but by following the work of Larchevêque [37],

$$\begin{cases} U_C = U_{Cc}\cos\beta \\ U_C = U_{Cs}\sin(\beta + \Lambda_{x/c}) \end{cases} \tag{5}$$

with $\Lambda_{x/c}$ the angle between the line of sensors at constant x/c and the y axis. Figure 16 shows a sketch with the variables defined here.

B. Frequency-Wave Number Spectra

The analysis of the frequency-wave number spectra is another way to compute the convection velocities. Theoretically, it is based on the two-dimensional Fourier transform of the spatiotemporal cross-correlation $R_{x_1x_2}(\Delta,\tau)$:

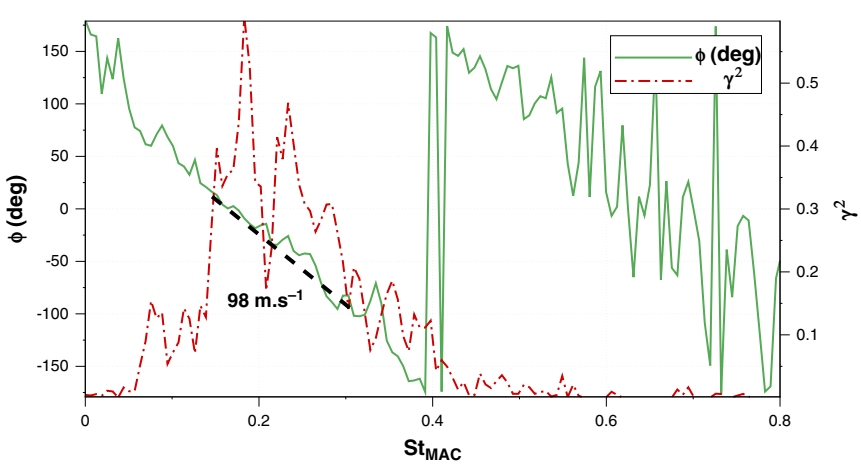

Fig. 15 Cross-spectrum coherence and phase at $x/c = 80\%$ on the suction side of the wing between two sensors at $y/b = 75\%$ and 95% for $\alpha = 3.5$ deg and $M = 0.82$ for BUFET'N Co test. The black dotted line is the slope considered in the buffet Strouhal number range 0.16–0.32 (defined thanks to buffet frequency map in Fig. 9) in order to compute the convection velocity.

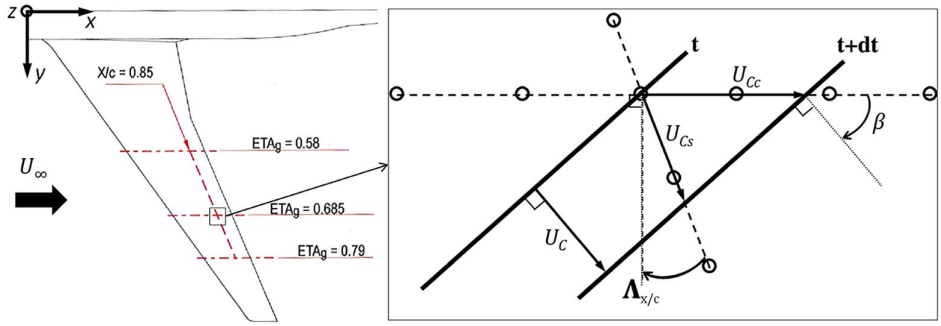

Fig. 16 Sketch of the measured velocity on the lines of sensors (dashed lines) in the chordwise U_{Cc} and in the spanwise U_{Cs} directions.

$$R_{x_1x_2}(\Delta,\tau) = \int_{-\infty}^{\infty}\int_{-\infty}^{\infty} x_1(x,t)x_2(x+\Delta,t+\tau)\,\mathrm{d}\tau\,\mathrm{d}\Delta \tag{6}$$

$$\hat{R}_{x_1x_2}(k,f) = \mathcal{F}\{R_{x_1x_2}(\Delta,\tau)\} \tag{7}$$

Since in space the definition of a transform is not possible because the sensors are not equidistant, an estimator $\psi(f,k)$ is defined. It is based on the cross-spectral matrix $\Psi(f)$ of the sensors (see [37] for more details),

$$\psi(k,f) = \eta^H(k)\Psi(f)\eta(k) \tag{8}$$

where H is the Hermitian transpose, k is the wave number, and $\eta(k)$ and $\Psi(f)$ are defined by

$$\begin{cases} (\Psi(f))_{ij} = \hat{R}_{x_ix_j}(f) \\ (\eta(k))_i = e^{-ikx_i} \end{cases} \tag{9}$$

The obtained estimator is a function of frequency and wave number. Convective phenomena are identified by regions of constant ratio ω/k, where ω is the pulsation and k is the wave number. The slope of these lines in the f–k plane corresponds to the convection velocity. Phase velocities ($U_p = 2\pi f/k$) are found with the cross-spectra, while in the f–k spectra, it is possible to find both phase and group velocities. The group velocity is the propagation of the real information of the waves, the envelope of a signal. It is defined as the variation of the angular frequency δf with the wave number, $U_g = 2\pi\delta f/\delta k$. The values of phase and group velocities found for 3D buffet are similar. A phenomenon with similar values of phase and group velocities is considered having low dispersion.

The results of f–k spectra are presented in the following paragraph. In all figures, the Strouhal number based on MAC is on the horizontal axis, and the dimensionless wave number is on the vertical axis (it has been divided by the chord or the span depending on the direction of the line of sensors analyzed). Figure 17 shows the results for one selected case of the BUFET'N Co test, and it is in complete agreement with the work of Dandois [14]. It is possible to identify the Kelvin–Helmholtz instability in the Strouhal number range 1–4 as well as the buffet phenomenon in the Strouhal number range 0.15–0.4. The magnitude of the velocity comes from the slope in the f–k spectrum $U_C = 2\pi\Delta f/\Delta k$. Both f–k spectra in the chordwise and in spanwise directions are shown, and the resulting velocity is obtained thanks to Eq. (5). In this case, the Kelvin–Helmholtz wave propagates mostly in the chordwise direction (indeed, it does not appear in the spanwise direction). The resulting velocity is typical of this instability, 180 $\mathrm{m\cdot s^{-1}}$ or $0.65U_\infty$ (see [14,38,39]). Concerning the buffet phenomenon, Fig. 17a gives a velocity of 90 $\mathrm{m\cdot s^{-1}}$, and Fig. 17b gives a velocity of 70 $\mathrm{m\cdot s^{-1}}$. The resulting buffet velocity has a norm of 66 $\mathrm{m\cdot s^{-1}}$ ($0.24U_\infty$) with $\beta = 43$ deg. The f–k spectra of BUFET'N Co show no convection velocities before buffet onset and the same results as in Fig. 17 at $\alpha = 3.3$ and 3.4 deg. The range of M–α tested is smaller than for the other campaigns, and it is not possible to look at the evolution of these velocities with M–α. This is not the case for the FLIRET and AVERT tests in which the M–α range is larger.

The f–k spectra of FLIRET differ a bit from BUFET'N Co since buffet convection velocity is more oriented toward the chordwise direction and K–H instability is convected not only in the chordwise but also in the spanwise direction. In the reference test at $M = 0.85$ and $\alpha = 3.37$ deg (Fig. 18), both the buffet and K–H instability velocities appear at $y/b = 79\%$ and in the chord at $x/c = 85\%$. Combining the velocities in the chord and span, the results are

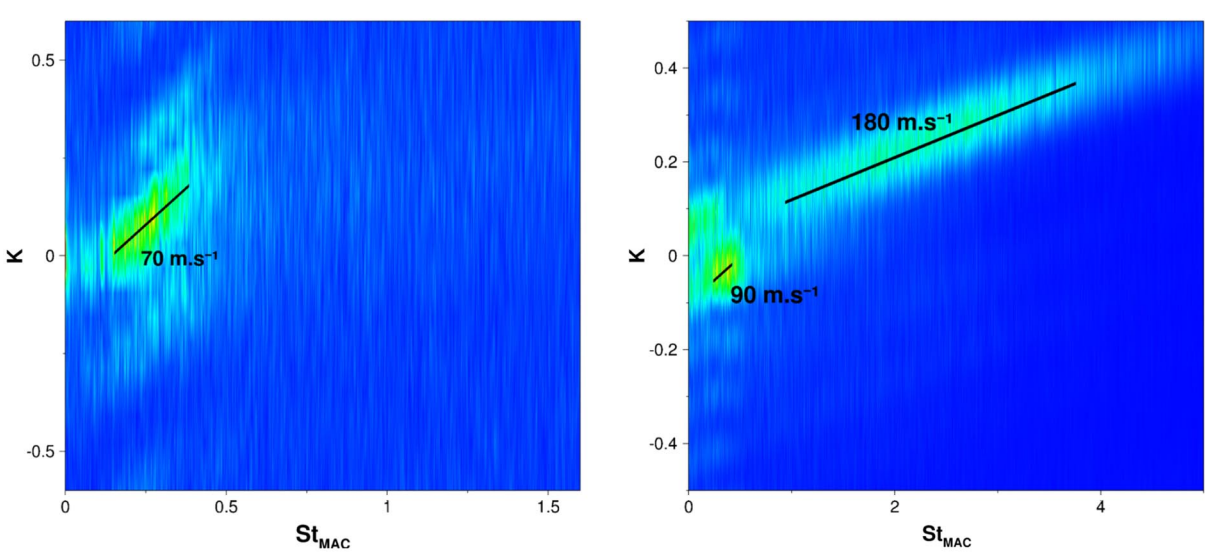

a) Spanwise direction at x/c=80% **b) Chordwise direction at y/b=60%**

Fig. 17 Frequency-wave number spectra for BUFET'N Co test at $\alpha = 3.5$ deg and $M = 0.82$.

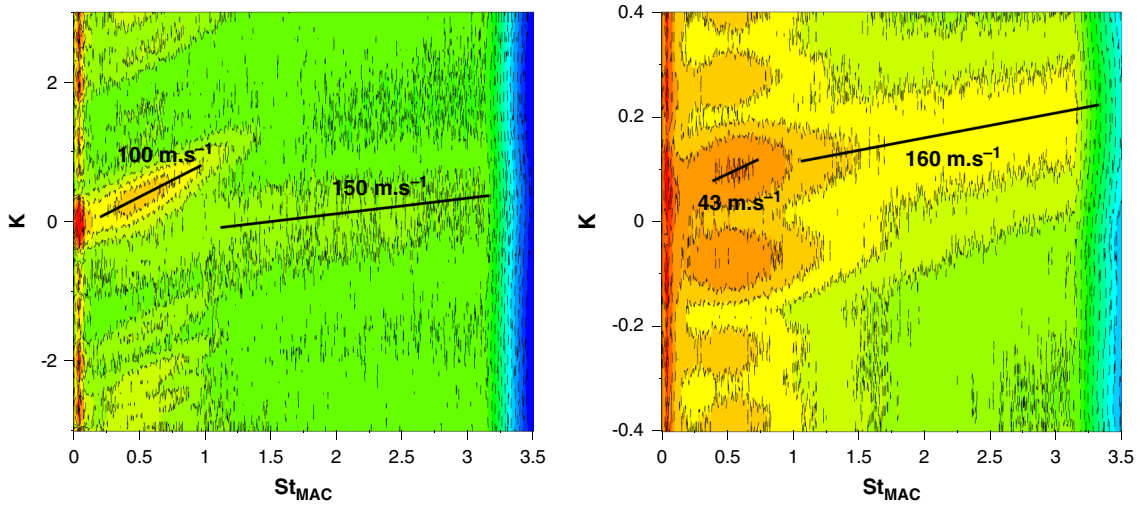

a) Spanwise direction at x/c = 85%

b) Chordwise direction at y/b=79%

Fig. 18 Frequency-wave number spectra for FLIRET test at $\alpha = 3.37$ deg and $M = 0.85$.

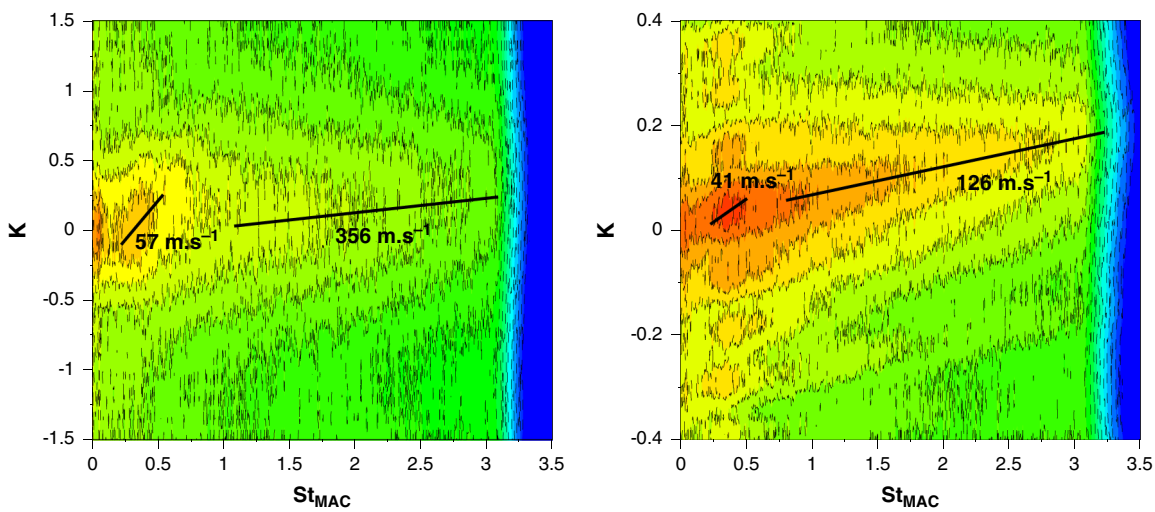

a) Spanwise direction at x/c = 85%

b) Chordwise direction at y/b=79%

Fig. 19 Frequency-wave number spectra for FLIRET test at $\alpha = 4.84$ deg and $M = 0.87$.

dimensionless convection velocities of $0.24U_\infty$ with $\beta = 2$ deg for the buffet and $0.63U_\infty$ with $\beta = 52$ deg for the K–H instability (the wind tunnel is cryogenic, so the velocities are lower, and just the dimensionless velocities are given here). Figure 19 shows other two f–k spectra at $\alpha = 4.84$ deg and $M = 0.87$ for the same position. Combining the velocities in the chord and span, the results are a dimensionless convection velocity for buffet of $0.2U_\infty$ with $\beta = 19$ deg and for a K–H instability of $0.61U_\infty$ with $\beta = 4$ deg. The effects of higher M–α are a K–H velocity more oriented toward the chordwise direction, while buffet convection velocity is more oriented in the spanwise direction toward the wing tip, and its norm is also slightly smaller than the typical value of $0.24U_\infty$.

The f–k spectra analysis for the AVERT test adds some interesting phenomena in comparison with the other databases and with the previous work of Dandois [14]. Above all, it is interesting to look at the precise evolution of the convection velocity for different angles of attack. The analysis is performed at a line position in the chord and span with the highest density of sensors Kulites and at a Mach number for which data are clearer and uniformly distributed in α. Figure 20 shows the f–k spectra in the chord and span (at x/c and y/b both 75%) for all the tests at a Mach number of 0.86. They represent the α evolution of the test: 0, 1.99, and 3.47 deg. For this value of the Mach number, the buffet onset is at $\alpha = 1$ deg (see Fig. 5b). In the following, only the final value and direction of the convection velocities by Eq. (5) are given. The analysis starts at $\alpha = 0$ deg (Figs. 20a and 20b), where it is possible to see two upstream convection velocities in both the chord and span. The first one is in the low Strouhal number range 0–0.3. It is a convection velocity at about 20 $\mathrm{m \cdot s^{-1}}$ ($0.07U_\infty$) with $\beta = 194$ deg, it corresponds to the propagation of a low-frequency acoustic wave, and indeed it is exactly equal to $U_{(x,\mathrm{wing})} - a$, where $U_{(x,\mathrm{wing})}$ is the chordwise velocity downstream of the shock and a is the speed of sound. The second velocity acts on a larger range of the Strouhal number 0.3–2.3, and it has a magnitude of about 180 $\mathrm{m \cdot s^{-1}}$ ($0.64U_\infty$) with $\beta = 250$ deg. It is also an acoustic wave; indeed, the same magnitude is found performing $U_{(s,\mathrm{wing})} - a$, where $U_{(s,\mathrm{wing})}$ is the velocity in the spanwise direction on the wing and a is the speed of sound. The two upstream acoustic waves are generated at the TE and the wing tip, respectively. Increasing α to 2 deg (Figs. 20c and 20d), there is a crucial point. Four different convection velocities appear in the chordwise f–k spectrum: the two upstream velocities described previously (with the same values of magnitude and direction) and two downstream convection velocities. The two downstream velocities are centered in the range of Strouhal number at 0.1–0.4 and 0.4–2.23, respectively. The low Strouhal convection velocity has a magnitude of 57 $\mathrm{m \cdot s^{-1}}$ ($0.21U_\infty$) and $\beta = 36$ deg. These values of the direction, magnitude and frequency range are consistent with a buffet convection velocity. The other downstream convection velocity appears only in the chord with a magnitude of 190 $\mathrm{m \cdot s^{-1}}$ ($0.65U_\infty$). The values of magnitude and the frequency range are consistent with

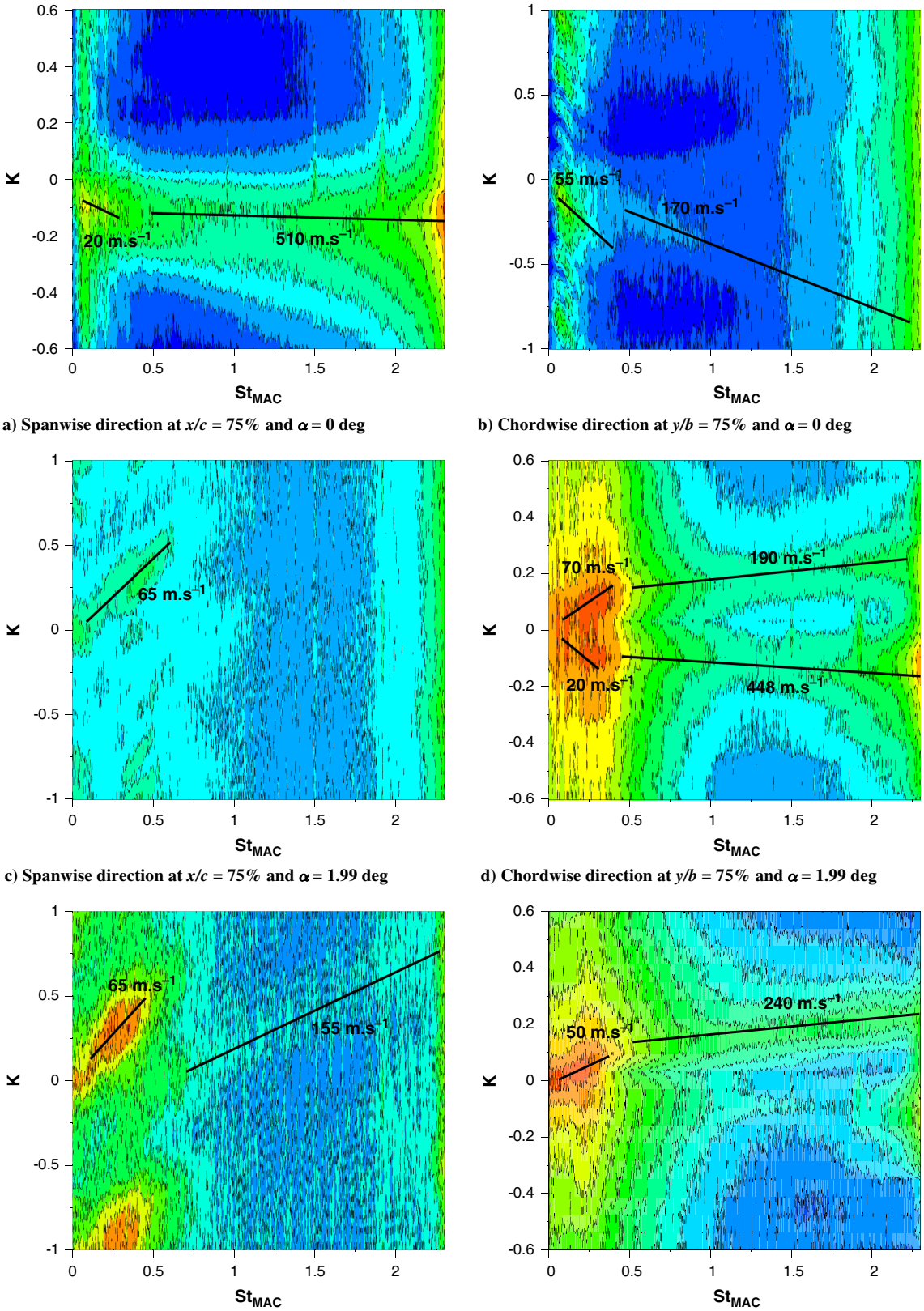

a) Spanwise direction at $x/c = 75\%$ and $\alpha = 0$ deg

b) Chordwise direction at $y/b = 75\%$ and $\alpha = 0$ deg

c) Spanwise direction at $x/c = 75\%$ and $\alpha = 1.99$ deg

d) Chordwise direction at $y/b = 75\%$ and $\alpha = 1.99$ deg

e) Spanwise direction at $x/c = 75\%$ and $\alpha = 3.47$ deg

f) Chordwise direction at $y/b = 75\%$ and $\alpha = 3.47$ deg

Fig. 20 Frequency-wave number spectra for AVERT test at $M = 0.86$.

a K–H convection velocity, and as in the BUFET'N Co database, it propagates mainly in the chordwise direction. When α reaches the values of 3.47 deg (Figs. 20e and 20f), only the two downstream velocities clearly appear in the spectra. It is still possible to discern an upstream high-frequency acoustic velocity in the chordwise direction (Fig. 20f) because acoustic velocities do not really disappear; they are just covered by other phenomena with larger amplitudes. The buffet convection velocity decreases: 48 $\mathrm{m \cdot s^{-1}}$ ($0.17U_\infty$) with $\beta = 20$ deg. The K–H convection velocity has a magnitude of 175 $\mathrm{m \cdot s^{-1}}$ ($0.63U_\infty$) and appears also in span with $\beta = 51$ deg, very close to the values and direction found for FLIRET in Fig. 18. Finally, at $\alpha = 5$ deg (not shown), the buffet velocity is

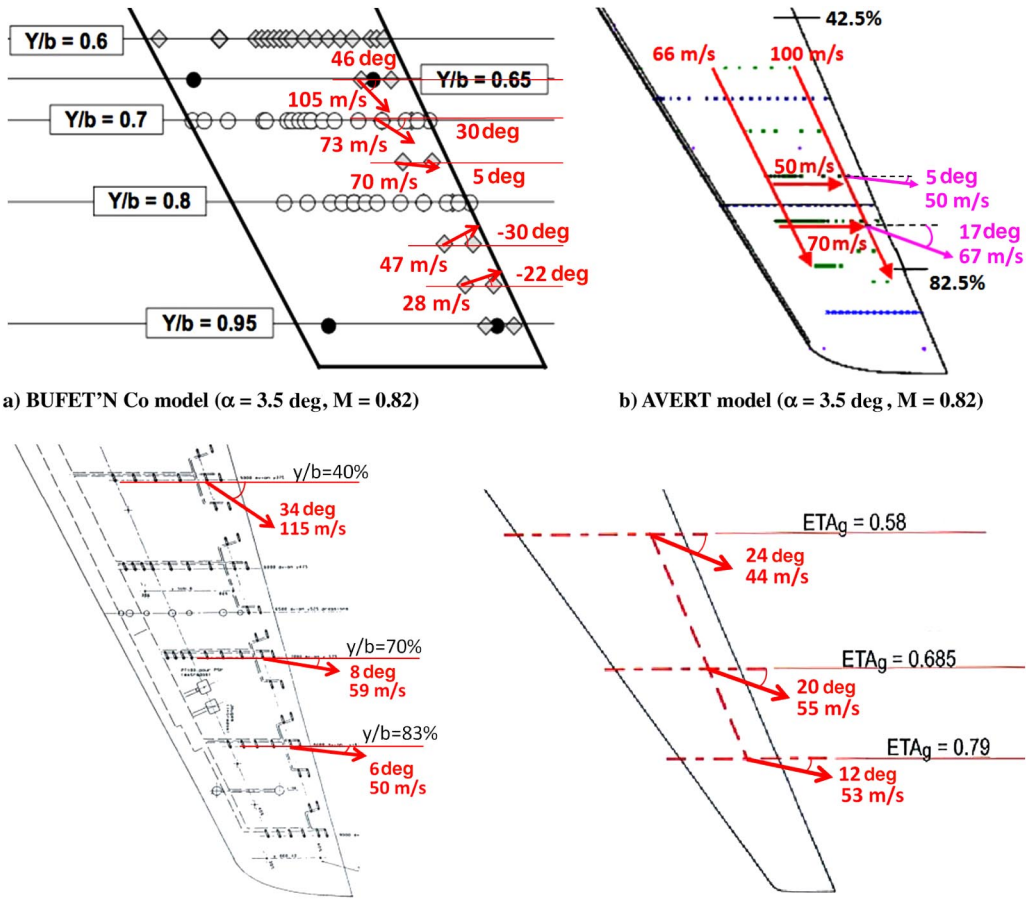

a) BUFET'N Co model (α = 3.5 deg, M = 0.82)

b) AVERT model (α = 3.5 deg , M = 0.82)

c) DTP Tremblement model (α = 4.3 deg, M = 0.8)

d) FLIRET model (α = 3.37 deg, M = 0.85)

Fig. 21 Buffet convection velocities for the four databases analyzed.

47 $\mathrm{m \cdot s^{-1}}$ ($0.17U_\infty$) with $\beta = 30$ deg, and the K–H instability velocity is 170 $\mathrm{m \cdot s^{-1}}$ ($0.6U_\infty$) with $\beta = 15$ deg. In summary, it seems that the buffet convection velocity decreases when the angle of attack increases.

C. Convection Velocities

The convection velocities are now presented at some characteristics points over the wings. The results of cross-spectra and f–k spectra are consistent with each other. For each wind-tunnel test, the cases considered are the most similar ones in terms of M–α: both BUFFET'N Co and AVERT at $M = 0.82$ and $\alpha = 3.5$ deg, FLIRET at $M = 0.85$ and $\alpha = 3.37$ deg, and DTP Tremblement at $M = 0.8$ and $\alpha = 4.3$ deg. The velocities found in chordwise and spanwise directions are combined following Eq. (5) and presented in Fig. 21 in dimensional units. Figure 21b also shows chordwise and spanwise velocity components.

All models exhibit buffet convection velocities in both the chordwise and spanwise directions. The convection in the span is characteristic of the 3D transonic buffet, and it is probably the main cause of the buffet cells convection toward the wing tip as identified by Iovnovich and Raveh [31]. FLIRET and BUFET'N Co show similar values of the convection velocities close to the trailing edge, about $0.26U_\infty$, while DTP Tremblement and AVERT have slightly lower values (0.235 ± 0.005 U_∞). The resulting dimensionless convection velocities are consistent with each other. Less consistency is found in the directions of the convections velocities, which are more dependent upon model geometry and position on the wing.

VII. Results Synthesis

Power spectral densities, cross-spectra, and frequency-wave number spectra of the unsteady pressure transducers as well as static pressure and accelerometers have been analyzed. The main results of the analysis of the four databases are summarized in Table 2, and they are essentially consistent with each other.

A. Strouhal Numbers and Convection Velocities Summary

It has been shown that 3D buffet appears with high-frequency values in comparison to two dimensions, especially for the well-established or deep buffet regime, while at the onset, peaks of PSDs are not so clear. Low-frequency peaks are found in some cases as in AVERT at $\alpha = 3$ deg and $M = 0.82$ (Fig. 22a). Figure 22b shows

Table 2 Summary of the main results for the four databases analyzed

Database	BUFET'N Co	AVERT	DTP Tremblement	FLIRET
Flow conditions	$\alpha = 3.5$ deg $M = 0.82$ x/c 80%, y/b 70%	$\alpha = 3.5$ deg $M = 0.82$ x/c 87.5%, y/b 75%	$\alpha = 4.3$ deg $M = 0.8$ x/c 80%, y/b 70%	$\alpha = 3.37$ deg $M = 0.85$ x/c 85%, y/b 79%
Onset	≈3 deg	≈3 deg	≈3.1 deg	≈3 deg
$St_{\mathrm{local}c}$	0.24	0.22	0.26	0.27
St_{MAC}	0.27	0.26	0.3	0.48
$St_{\mathrm{MAC}'}$	— —	— —	0.23	0.33
U_C/U_∞	0.26	0.24	0.23	0.26

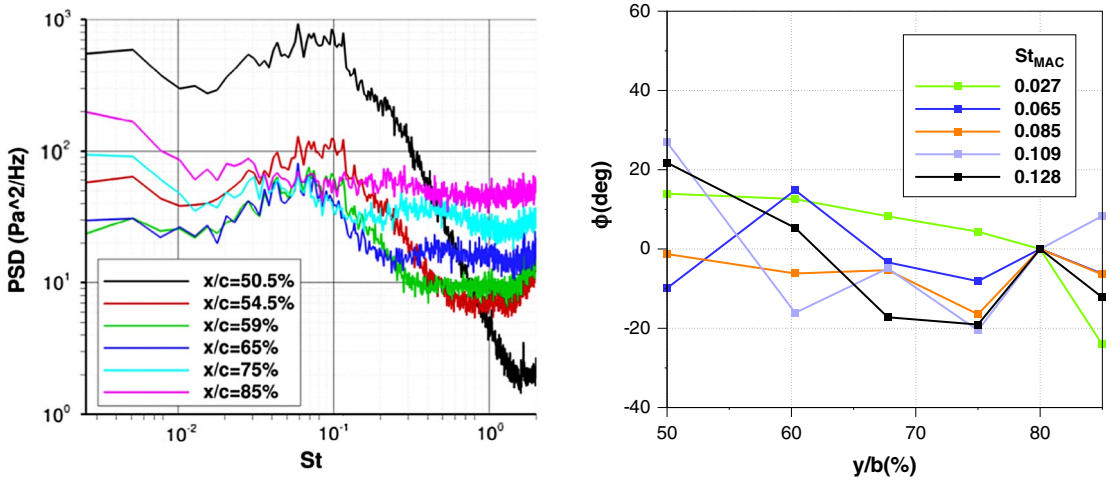

a) Power spectral densities for different chordwise locations at *y/b* = 75%; Strouhal number is based on MAC from [14]

b) Phase of cross-spectra at *x/c* = 85% for five selected frequencies (reference sensor: *y/b* = 80%)

Fig. 22 AVERT test at $M = 0.82$ and $\alpha = 3$ deg.

the resulting phase from cross-spectra at five selected frequencies (the only ones with high coherence): the buffet phenomenon is more 2D than 3D, and indeed there is nearly no phase difference in the span, and no convection velocity is found. The convection in the spanwise direction is probably the key of the difference between 2D and 3D buffet. There is a switch from 2D to 3D buffet only with the presence of this convection in span.

The buffet Strouhal number strongly varies on the wing in the well-established regime while remaining more constant at onset and in deep buffet. The way it varies on the different models is almost the same: the Strouhal number decreases in the chordwise direction toward the TE and in the spanwise direction toward the wing tip. The Strouhal number values are consistent between the different models. The best way to compare the models is probably to use the local Strouhal number because of the different taper ratios (0.83 for BUFET'N Co, 0.5 for AVERT, 0.3 for DTP Tremblement, and 0.21 for FLIRET). Good agreement is also found when considering MAC′ as a reference length, for which the Strouhal numbers are in the same range of 0.2–0.3. The decrease of the Strouhal number with α is also a common effect (Fig. 10c, Fig. 12, Sartor and Timme [32], and Sugioka et al. [17]), while the tendency with the Mach number is less clear and needs further study. Furthermore, a convective behavior is found at the buffet Strouhal number on the wing for all models. The values of dimensionless convection velocities are consistent with each other, and a typical range of values $(0.245 \pm 0.015)U_\infty$ can be defined. These values are smaller than the spanwise component of the freestream velocity $[U_\infty \sin(\Lambda) \approx 0.5U_\infty]$. Finally, a spanwise convection of buffet cells is found (except for DTP Tremblement because it is unavailable), which confirms what has been observed by Iovnovich and Raveh [31]. This phenomenon has been presented in the Introduction, and it will be better analyzed in the next paragraph.

B. Buffet Cell Wavelengths Summary

The discovery of a convective phenomenon of so-called buffet cells in the spanwise direction on a wing during buffet is very recent. As already mentioned in the Introduction, Iovnovich and Raveh [31] were the first to observe this convection numerically in 2015 and introduce the name *buffet cells*. Dandois [14] computed the convection velocity on the AVERT model by using a cross-spectrum analysis. From the values of the phase difference, it is possible to define the wavelength of the cells λ. For the AVERT project, two different values of λ/MAC are found: 1.6 for $\alpha = 3.5$ deg and 1.3 for $\alpha = 4.25$ deg. Figure 23 shows the phase differences in the spanwise direction at the buffet Strouhal number for the flow conditions: $M = 0.82$ and $\alpha = 3.5$ deg for BUFET'N Co and $M = 0.85$ and $\alpha = 3.6$ deg for FLIRET. This information may then be translated into wavelengths characterizing the buffet cells $\lambda = U_C/f = 2\pi\Delta x/\Delta\varphi$. Table 3 shows all the values of wavelengths computed and a comparison with [31]. Wavelengths are

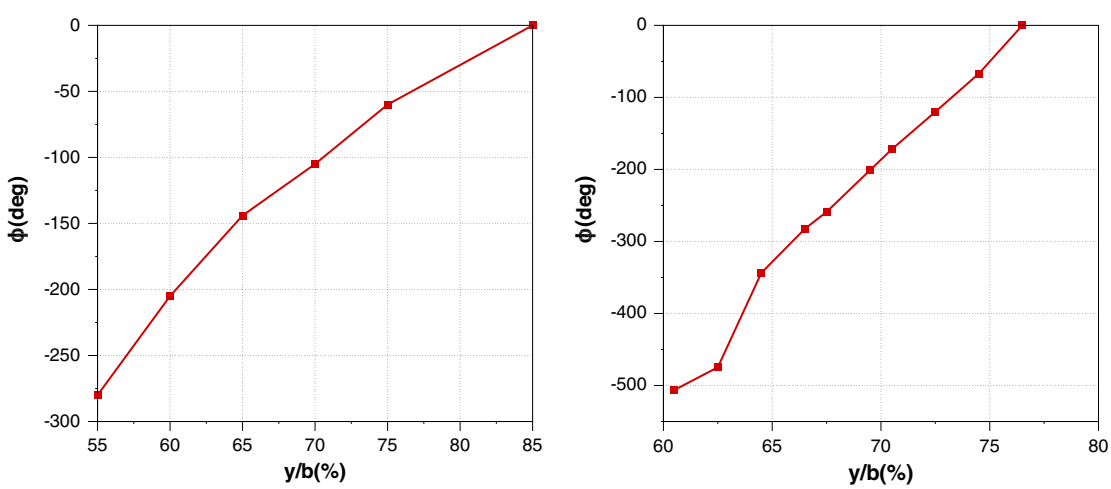

a) Values at *x/c* = 80%, St_{MAC} = 0.26, *M* = 0.82, and α = 3.5 deg for BUFET'N Co model (reference sensor at *y/b* = 85%)

b) Values at *x/c* = 85%, $St_{MAC'}$ = 0.33, *M* = 0.85, and α = 3.6 deg for FLIRET model (reference sensor at *y/b* = 76.5%)

Fig. 23 Phase of cross-spectra along the span.

Table 3 Dimensionless wavelength for the convective buffets cells

Database	BUFET'N Co	AVERT	FLIRET	Iovnovich and Raveh [31] $\Lambda = 30$ deg
Flow conditions	$M = 0.82$	$M = 0.82$	$M = 0.85$	$M\cos(\Lambda) = 0.73$
λ/MAC	0.56 at $\alpha = 3.5$ deg	1.3 at $\alpha = 4.25$ deg	0.62 at $\alpha = 3.6$ deg	1.3 at $\alpha = 4$ deg
	— —	1.6 at $\alpha = 3.5$ deg	0.55 at $\alpha = 3.8$ deg	— —
λ/MAC'	0.56 at $\alpha = 3.5$ deg	1.6 at $\alpha = 3.5$ deg	0.9 at $\alpha = 3.6$ deg	1.3 at $\alpha = 4$ deg
λ/c (at $y/b = 78\%$)	0.7 at $\alpha = 3.5$ deg	1.9 at $\alpha = 3.5$ deg	1.2 at $\alpha = 3.5$ deg	1.3 at $\alpha = 4$ deg

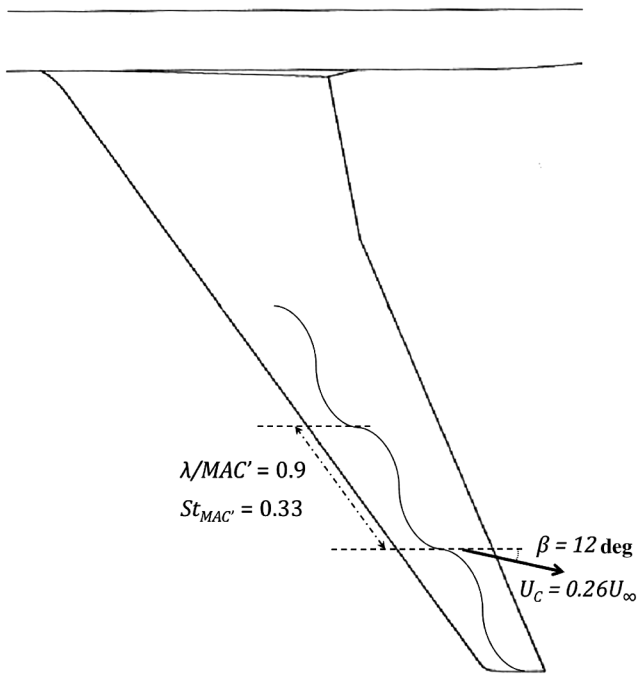

Fig. 24 Buffet cells convection on FLIRET model at $\alpha = 3.6$ deg and $M = 0.85$.

presented here as dimensionless numbers. It is possible to state that the wavelength decreases with the angle of attack but its value depends on the wing geometry. Finally, even if the geometrical dependency is very high, it is still possible to define a range of λ/MAC between 0.6 and 1.3 for these supercritical wings.

To conclude this overview, Fig. 24 shows a sketch of the buffet cells convection for the FLIRET model. The values of wavelength and Strouhal number are presented with MAC′ as a reference length together with the buffet convection velocity.

VIII. Conclusions

The present Paper compares the buffet phenomenon characteristics (Strouhal number and convection velocity) on four different databases. The models are different in terms of the chord length, taper ratio, twist, and geometry, but they are all based on supercritical airfoils. Two main results have been obtained. The first one is the characterization of all the convection velocities of the phenomena propagating on the suction side of four different wings. This study shows that buffet is a strongly convective phenomenon in three dimensions, and the values found are consistent for the different models. A characteristic convection velocity range of $(0.245 \pm 0.015)U_\infty$ is found for a sweep angle of 30 deg. It has been shown that these velocities are the main cause of the buffet cells convecting in the spanwise direction. The second main result is the definition of a frequency range of the buffet phenomenon. A range of Strouhal numbers based on the local chord of 0.2–0.3 is found. It is important to underline the difference with [14] (of which this article is the continuation). Here, the analysis is more oriented toward the variability of the phenomenon in the different databases and its sensibility with respect to the different configurations.

Finally, a comparison between 2D and 3D transonic buffet is assessed. The increase of the frequency [31], the change of shock amplitude oscillation, and the creation of buffet cells are not still completely understood, but the convection of buffet cells in the spanwise direction of the wing is the main difference between the two types of buffet. It is crucial in three dimensions to look for the existence or lack of existence of an unstable global mode as found by Crouch et al. [6] in two dimensions. Indeed, the spanwise convective nature of the 3D transonic buffet does not rule out the possibility of explaining it with a global mode as in two dimensions; the broadband nature of the spectra stems from unmodeled noise [40]. The second hypothesis is a convective instability in which the convection velocities wipe out the presence of an unstable global mode and establish a noise-amplifier behavior. A challenging 3D global stability analysis could state which hypothesis is closer to 3D transonic buffet. The only 3D global analysis performed until now by Timme and Thormann [10] does not really answer the question. Indeed, the analysis has been performed only at low value of α, and just the emergence of some destabilizing global modes approaching the imaginary axis is found. Repeating the 3D global stability analysis with this point of view is a future main goal.

Acknowledgments

The AVERT S2MA wind-tunnel tests were conducted within the FP7 AVERT European project (contract number AST5-CT-2006-030914), funded by the European Commission and project partners (Airbus Operations, Ltd.; Airbus Operations SL; Dassault Aviation; Alenia Aeronautica; and ONERA). The S3Ch wind-tunnel tests have been performed in the framework of ONERA's joint research project BUFET'N Co. devoted to buffet control on a transonic three-dimensional wing using a closed-loop approach. The European Transonic Windtunnel tests were conducted within the FP6 FLIRET European project (contract number AIP3-CT-2003-502773), funded by the European Commission. Concerning the DTP Tremblement project, the authors gratefully acknowledge the DGAC from the French Ministry of Transport, which granted the research reported in this Paper.

References

[1] Lee, B., "Oscillatory Shock Motion Caused by Transonic Shock Boundary-Layer Interaction," *AIAA Journal*, Vol. 28, No. 5, 1990, pp. 942–944.
doi:10.2514/3.25144

[2] Deck, S., "Numerical Simulation of Transonic Buffet over a Supercritical Airfoil," *AIAA Journal*, Vol. 43, No. 7, 2005, pp. 1556–1566.
doi:10.2514/1.9885

[3] Memmolo, A., Bernardini, M., and Pirozzoli, S., "Scrutiny of Buffet Mechanisms in Transonic Flow," *International Journal of Numerical Methods for Heat & Fluid Flow*, Vol. 28, No. 5, 2018, pp. 1031–1046.

[4] Xiao, Q., Tsai, H., and Liu, F., "Numerical Study of Transonic Buffet on a Supercritical Airfoil," *AIAA Journal*, Vol. 44, No. 3, 2006, pp. 620–628.
doi:10.2514/1.16658

[5] Jacquin, L., Molton, P., Deck, S., Maury, B., and Soulevant, D., "Experimental Study of Shock Oscillation over a Transonic Supercritical Profile," *AIAA Journal*, Vol. 47, No. 9, 2009, pp. 1985–1994.
doi:10.2514/1.30190

[6] Crouch, J., Garbaruk, A., and Magidov, D., "Predicting the Onset of Flow Unsteadiness Based on Global Instability," *Journal of*

Computational Physics, Vol. 224, No. 2, 2007, pp. 924–940. doi:10.1016/j.jcp.2006.10.035

[7] Crouch, J., Garbaruk, A., Magidov, D., and Travin, A., "Origin and Structure of Transonic Buffet on Airfoils," *Journal of Fluid Mechanics*, Vol. 628, June 2009, pp. 357–369. doi:10.1017/S0022112009006673

[8] Sartor, F., Mettot, C., and Sipp, D., "Stability, Receptivity, and Sensitivity Analyses of Buffeting Transonic Flow over a Profile," *AIAA Journal*, Vol. 53, No. 7, 2015, pp. 1980–1993. doi:10.2514/1.J053588

[9] Guiho, F., "Analyse de Stabilité Linéaire Globale d'Écoulements Compressibles: Application aux Interactions onde de choc/Couche Limite," Ph.D. Thesis, ENSAM, Paris, 2015.

[10] Timme, S., and Thormann, R., "Towards Three-Dimensional Global Stability Analysis of Transonic Shock Buffet," *AIAA Atmospheric Flight Mechanics Conference*, AIAA Paper 2016-3848, 2016.

[11] Reneaux, J., Brunet, V., Caruana, D., Deck, S., and Naudin, P., "A Combined Experimental and Numerical Investigation of the Buffet Phenomenon and Its Control Through Passive and Active Devices," *CEAS Katnet Conference on Key Aerodynamic Technologies*, June 2005.

[12] Roos, F., "The Buffeting Pressure Field of a High-Aspect-Ratio Swept Wing," *18th Fluid Dynamics and Plasma Dynamics and Lasers Conference*, AIAA Paper 1985-1609, July 1985.

[13] Molton, P., Dandois, J., Lepage, A., Brunet, V., and Bur, R., "Control of Buffet Phenomenon on a Transonic Swept Wing," *AIAA Journal*, Vol. 51, No. 4, 2013, pp. 761–772. doi:10.2514/1.J051000

[14] Dandois, J., "Experimental Study of Transonic Buffet Phenomenon on a 3D Swept Wing," *Physics of Fluids*, Vol. 28, No. 1, 2016, pp. 1–22. doi:10.1063/1.4937426

[15] McDevitt, J. B., and Okuno, A. F., "Static and Dynamic Pressure Measurements on a NACA 0012 Airfoil in the Ames High Reynolds Number Facility," NASA TP-2485, 1985.

[16] Iovnovich, M., and Raven, D. E., "Reynolds-Averaged Navier-Stokes Study of the Shock-Buffet Instability Mechanism," *AIAA Journal*, Vol. 50, No. 4, 2012, pp. 880–890. doi:10.2514/1.J051329

[17] Sugioka, Y., Numata, D., Asai, K., Koike, S., Nakakita, K., and Koga, S., "Unsteady PSP Measurement of Transonic Buffet on a Wing," *53rd AIAA Aerospace Science Meeting*, AIAA Paper 2015-0025, 2015. doi:10.2514/6.2015-0025

[18] Lawson, S. G., Greenwell, D., and Quinn, M., "Characterisation of Buffet on a Civil Aircraft Wing," *54th AIAA Aerospace Science Metting*, AIAA Paper 2016-1309, 2016. doi:10.2514/6.2016-1309

[19] Koike, S., Ueno, M., Nakakita, K., and Hashimoto, A., "Unsteady Pressure Measurement of Transonic Buffet on NASA Common Research Model," *34th AIAA Applied Aerodynamics Conference*, AIAA Paper 2016-4044, 2016. doi:10.2514/6.2016-4044

[20] Hwang, C., and Pi, W., "Northrop F-5A Aircraft Transonic Buffet Pressure Data Acquisition and Response Analysis," *Journal of Aircraft*, Vol. 12, No. 9, 1975, pp. 714–720. doi:10.2514/3.44487

[21] Eckstrom, C. V., Seidel, D. A., and Sandford, M. C., "Unsteady Pressure and Structural Response Measurements on an Elasticsupercritical Wing," *Journal of Aircraft*, Vol. 27, No. 1, 1990, pp. 75–80. doi:10.2514/3.45898

[22] Eckstrom, C. V., Seidel, D. A., and Sandford, M. C., "Measurements of Unsteady Pressure and Structural Response for an Elastic Supercritical Wing," NASA TP 3443, 1994.

[23] Steimle, C., Karhoff, D.-C., and Schröder, W., "Unsteady Transonic Flow over a Transport-Type Swept Wing," *AIAA Journal*, Vol. 50, No. 2, 2012, pp. 399–415. doi:10.2514/1.J051187

[24] Merienne, M.-C., Le Sant, Y., Lebrun, F., Deleglise, B., and Sonnet, D., "Transonic Buffeting Investigation Using Unsteady Pressure-Sensitive Paint in a Large Wind Tunnel," *51st AIAA Aerospace Science Meeting*, AIAA Paper 2013-1136, 2013. doi:10.2514/6.2013-1136

[25] Masini, L., Timme, S., Ciarella, A., and Peace, A., "Influence of Vane Vortex Generators on Transonic Wing Buffet: Further Analysis of the BUCOLIC Experimental Dataset," *Proceedings of the 52nd 3AF International Conference on Applied Aerodynamics*, French Aeronautics and Astronautics Soc. Paper FP14-AERO2017-masini, Lyon, France, 2017.

[26] Giannelis, N. F., Vio, G. A., and Levinski, O., "A Review of Recent Developments in the Understanding of Transonic Shock Buffet," *Progress in Aerospace Sciences*, Vol. 92, July 2017, pp. 39–84. doi:10.1016/j.paerosci.2017.05.004

[27] Brunet, V., and Deck, S., "Zonal-Detached Eddy Simulation of Transonic Buffet on a Civil Aircraft Type Configuration," *38th Fluid Dynamics Conference and Exhibit*, AIAA Paper 2008-4152, 2008. doi:10.2514/6.2008-4152

[28] Deck, S., "Recent Improvements in the Zonal Detached Eddy Simulation (ZDES) Formulation," *Theoretical and Computational Fluid Dynamics*, Vol. 26, No. 6, 2012, pp. 523–550. doi:10.1007/s00162-011-0240-z

[29] Deck, S., Gand, F., Brunet, V., and Khelil, S. B., "High-Fidelity Simulations of Unsteady Civil Aircraft Aerodynamics: Stakes and Perspectives. Application of Zonal Detached Eddy Simulation," *Philosophical Transactions of the Royal Society A: Mathematical, Physical and Engineering Sciences*, Vol. 372, No. 2022, 2014, pp. 1–21. doi:10.1098/rsta.2013.0325

[30] Lutz, T., Gansel, P. P., Waldmann, A., Zimmermann, D., and Schulte am Hülse, S., "Prediction and Measurement of the Common Research Model Wake at Stall Conditions," *Journal of Aircraft*, Vol. 53, No. 2, 2016, pp. 501–514. doi:10.2514/1.C033351

[31] Iovnovich, M., and Raveh, D. E., "Numerical Study of Shock Buffet on Three-Dimensional Wings," *AIAA Journal*, Vol. 53, No. 2, 2015, pp. 449–463. doi:10.2514/1.J053201

[32] Sartor, F., and Timme, S., "Reynolds-Averaged Navier-Stokes Simulations of Shock Buffet on Half Wing-Body Configuration," *53rd AIAA Aerospace Sciences Meeting*, AIAA Paper 2015-1939, 2015. doi:10.2514/6.2015-1939

[33] Sartor, F., and Timme, S., "Delayed Detached-Eddy Simulation of Shock Buffet on Half Wing-Body Configuration," *22nd AIAA Computational Fluid Dynamics Conference*, AIAA Paper 2015-2607, 2015. doi:10.2514/6.2015-2607

[34] Pearcey, H. H., Osborne, J., and Haines, A. B., "The Interaction Between Local Effects at the Shock and Rear Separation—A Source of Significant Scale Effects in Wind-Tunnel Tests on Aerofoils and Wings," AGARD TR CP-35, National Physics Lab., United Kingdom, 1968.

[35] Mundell, A. R. G., and Mabey, D. G., "Pressure Fluctuations Caused by Transonic Shock/Boundary-Layer Interaction," *Aeronautical Journal*, Vol. 90, No. 897, 1986, pp. 274–282. doi:10.1017/S0001924000015864

[36] Huerre, P., and Rossi, M., "Hydrodynamic Instabilities in Open Flows," *Collection Alea Saclay Monographs and Texts in Statistical Physics*, Vol. 1, No. 3, 1998, pp. 81–294.

[37] Larchevêque, L., "Simulation des Grandes Échelles de l'Écoulement au-dessus d'une Cavité," Ph.D. Thesis, Université Pierre et Marie Curie, Paris, 2003.

[38] Dandois, J., Garnier, E., and Sagaut, P., "Numerical Simulation of Active Separation Control by a Synthetic Jet," *Journal of Fluid Mechanics*, Vol. 574, March 2007, pp. 25–58. doi:10.1017/S0022112006003995

[39] Larchevêque, L., Sagaut, P., Le, T., and Comte, P., "Large-Eddy Simulation of a Compressible Flow in a Three-Dimensional Open Cavity at High Reynolds Number," *Journal of Fluid Mechanics.*, Vol. 516, Oct. 2004, pp. 265–301. doi:10.1017/S0022112004000709

[40] Bagheri, S., "Effects of Weak Noise on Oscillating Flows: Linking Quality Factor, Floquet Modes, and Koopman Spectrum," *Physics of Fluids*, Vol. 26, No. 9, 2014, pp. 1–17. doi:10.1063/1.4895898

D. E. Raveh
Associate Editor